Chronic exposure to odors at naturally occurring concentrations triggers limited plasticity in early stages of *Drosophila* olfactory processing

Zhannetta V. Gugel, Elizabeth Maurais, and Elizabeth J. Hong*

Division of Biology and Biological Engineering, California Institute of Technology, Pasadena, CA

*Correspondence to ejhong@caltech.edu

ABSTRACT

In insects and mammals, chronic exposure to odors at high concentrations in early life alters olfactory function, but the role of odor experience-dependent plasticity in more naturalistic contexts is less clear. We investigated olfactory plasticity in the *Drosophila* antennal lobe by exposing flies to odors at concentrations that are typically encountered in natural odor sources. These stimuli also strongly and selectively activated only a single class of olfactory receptor neuron (ORN) input, facilitating the investigation of input-specific plasticity. Overall, chronic exposure to three such odors elicited limited plasticity in the odor responses of second-order projection neurons (PNs). Exposure to some odors elicited mild increases in PN responses to weak stimuli, extending the lower bound of the dynamic range of PN signaling. When present, plasticity was observed broadly in multiple PN types and thus was not selective for PNs receiving direct input from the chronically active ORNs. Chronic E2-hexenal exposure did not affect PN intrinsic properties, local inhibitory innervation, ORN responses, or ORN-PN synaptic strength, but modestly increased broad lateral excitation evoked by some odors. These results show that PN odor coding is only mildly affected by strong persistent activation of a single olfactory input and highlight the stability of early stages of insect olfactory processing to significant perturbations in the sensory environment.

INTRODUCTION

In many animals, early sensory experience modifies the structure and function of sensory circuits. For example, the requirement for visual experience in the development of mammalian visual system function is well studied (Espinosa and Stryker, 2012). One prominent hypothesis in this field is that sensory plasticity may adapt circuit function to the current statistical distribution of sensory inputs in the environment, allowing for more efficient sensory codes (*5–23*)(Barlow, 1961; Fiser et al., 2010; Gilbert et al., 2009; Pienkowski and Eggermont, 2011). This hypothesis requires that sensory driven plasticity be stimulus- and cell-specific; in other words, neurons encoding specific stimuli that occur very frequently (or very rarely) in the environment should be selectively affected by plasticity (Das et al., 2011; Kreile et al., 2011; Sachse et al., 2007; Sengpiel et al., 1999; Wilson et al., 1985; Zhang et al., 2001).

The orderly structure of the olfactory system provides a useful experimental model for investigating the synaptic and circuit mechanisms mediating stimulus-selective sensory plasticity. In insect and vertebrate olfactory circuits, sensory information is organized in anatomically discrete synaptic units, called glomeruli. Each glomerulus receives direct input from only a single class of primary olfactory receptor neurons (ORNs), all expressing the same olfactory receptor, and, thus, all sensitive to the same chemical feature(s) (Ressler et al., 1994; Vassar et al., 1994; Vosshall and Stocker, 2007; Vosshall et al., 2000). Furthermore, the dendrites of each second-order uniglomerular projection neuron (PN) arborize in only a single glomerulus, so each PN receives direct input from only a single class of ORNs (Stocker et al., 1990). In the vinegar fly *Drosophila melanogaster*, the majority of odorant receptors and ORN subtypes have been mapped to their cognate glomeruli in the brain (Couto et al., 2005; Fishilevich and Vosshall, 2005; Silbering et al., 2011), and the odor tuning profiles for a large subset of the odorant receptors have been characterized (de Bruyne et al., 1999, 2001; Hallem and Carlson, 2006;

Hallem et al., 2004; Silbering et al., 2011). As a result, specific odors can be used to selectively target neural activation of defined olfactory channels (Olsen et al., 2010; Schlief and Wilson, 2007). Together with the highly compartmentalized organization of the circuit, these features make the fly olfactory system a powerful experimental model for studying the specificity of sensory plasticity.

Passive odor experience in early life, in the absence of explicit coupling to reward or punishment, can alter olfactory circuit structure and function, including olfactory preference or discrimination ability (Mandairon and Linster, 2009; Mandairon et al., 2006a). In contrast to the mammalian visual system, where early stages of sensory processing are mostly unaffected by large perturbations in the visual environment (D'Orazi et al., 2014; Elstrott and Feller, 2009), the olfactory system appears to exhibit plasticity at the earliest stages of processing. For instance, chronic odor exposure in rodents can trigger changes in the structural connectivity and physiological response properties of neurons in the olfactory bulb, the first central processing area for odors in the brain (Liu and Urban, 2017; Liu et al., 2016; Todrank et al., 2011; Wilson et al., 1985; Woo et al., 2006). Odor exposure-driven plasticity can occur as early in processing as in the peripheral olfactory sensory neurons, and includes changes in their number, sensitivity, and tuning, although the direction of these effects varies in different studies (Cadiou et al., 2014; Cavallin et al., 2010; Jones et al., 2008; Kass et al., 2013; Santoro and Dulac, 2012; Wang et al., 1993; Watt et al., 2004).

In insects, passive odor experience also impacts early olfactory processing in the antennal lobe, the insect analog of the olfactory bulb (Golovin and Broadie, 2016). Like in vertebrates, no common set of principles has emerged to predict how exposure to a specific odor environment impacts olfactory system function. For instance, chronic exposure of *Drosophila* to odors has been reported to either decrease (Das et al., 2011; Devaud et al., 2001, 2001; Sachse et al., 2007) or increase (Chakraborty et al., 2009) behavioral responses to the

odor; decrease (Devaud et al., 2001, 2003; Golovin et al., 2019) or increase (Das et al., 2011; Kidd et al., 2015; Sachse et al., 2007) glomerular volume; and decrease (Das et al., 2011; Pech et al., 2015; Sachse et al., 2007) or increase (Kidd and Lieber, 2016; Kidd et al., 2015) the strength of second-order PN odor responses. Most studies in insects report that behavioral, structural, and physiological changes induced by odor exposure are stimulus-specific. In other words, changes in behavior are selective for the exposure odor and do not generalize to other odors. Likewise, structural and physiological changes are observed only in some glomeruli, in a way that depends on the identity of the odor used for chronic exposure (Chakraborty et al., 2009; Das et al., 2011; Devaud et al., 2001, 2003; Sachse et al., 2007).

A systematic understanding of how odor experience modifies the structure and function of olfactory circuits has been difficult to achieve for several reasons. First, diverse protocols are used for odor exposure, which vary in the degree of control over odor delivery, odor concentration, timing, as well as context (availability of food, mates, etc). Second, different studies focus on different odors and glomeruli, and the high dimensionality of olfactory stimuli and olfactory circuits presents unique challenges to methodical exploration. As a consequence, past work has come to diverse, sometimes divergent, conclusions about the impact of long-term odor exposure on olfactory circuits. Finally, nearly all studies, in insects or in rodents, use very high concentrations of monomolecular odorants during the exposure period, at intensities that are not encountered in the natural word (see Discussion). Odors at these concentrations broadly activate many classes of ORNs, complicating the evaluation of the contributions of direct and indirect activity for triggering plasticity in each olfactory processing channel. Some of the major outstanding questions include: 1) How does olfactory plasticity modify circuit function in the context of odor environments that could be realistically encountered in the natural world? 2) To what extent is plasticity selective for the olfactory channel(s) which directly detect

overrepresented odors? 3) Are the rules governing olfactory plasticity the same or different across glomeruli?

The goals of this study were to investigate the impact of olfactory experience on odor coding in the *Drosophila* antennal lobe, using a physiologically plausible olfactory environment that strongly but selectively increases neural activity in a single class of ORNs. This experimental design allowed us to readily distinguish the effects of direct versus indirect chronic activity on specific classes of PNs, which convey neural output from the antennal lobe to higher olfactory centers in the fly brain. This distinction is important because it allowed us to unambiguously evaluate whether olfactory plasticity affects specifically only the chronically active glomerulus. Investigating three different glomerular channels, we observed that strong perturbation of olfactory inputs during the early life of the fly had a relatively mild effect on antennal lobe circuitry. A limited amount of plasticity was observed in the responses of PNs to weak odors, extending the lower bound of the dynamic range for PN signaling. Changes in odor responses, when present, were observed broadly, both in glomeruli that receive either direct or indirect activity from the chronically activated ORN class. ORN odor responses, ORN-PN synaptic strength, and PN intrinsic properties were stable and unchanged by chronic odor exposure. These results diverge from current models suggesting that odor-specific behavioral plasticity stems from glomerulus-specific neural plasticity in the antennal lobe (Das et al., 2011; Kidd et al., 2015; Sachse et al., 2007).

RESULTS

Chronic activation of direct ORN input modestly increases PN responses to weak stimuli

120 To investigate how odors that are overrepresented in the flies' environment are encoded
121 by the olfactory system, we chronically exposed flies to 1 sec pulses of a specific monomolecular
122 odorant, introduced into the bottle in which they normally grow (Figure 1A). We chose to use the

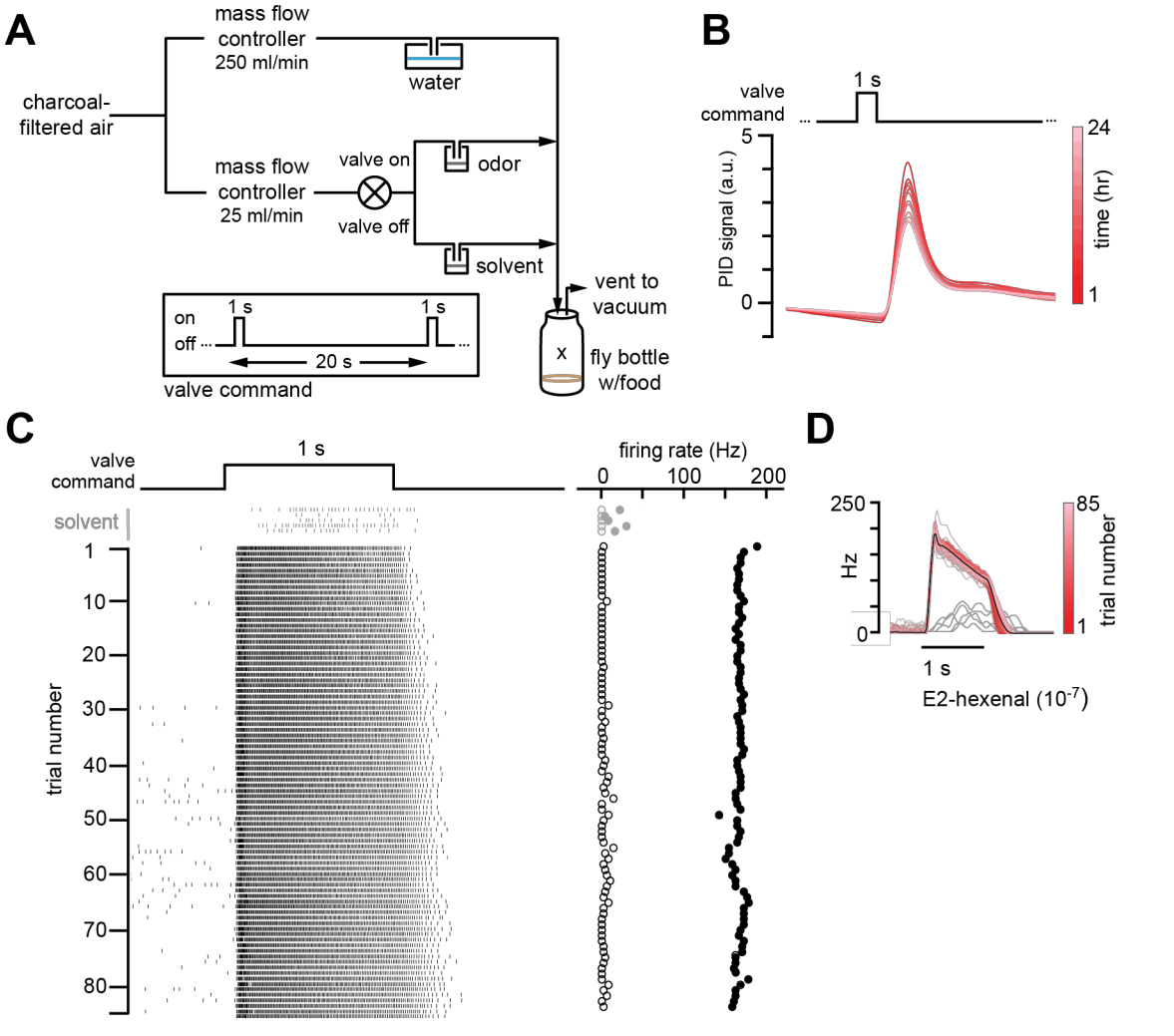

Figure 1: Chronic stimulation of olfactory neurons in a controlled odor environment.
A) Schematic of experimental setup for chronic odor exposure. The valve was opened for 1 s every 20 s to deliver odor. See **Methods** (*Chronic Odor Exposure*) for details.
B) Photoionization detector measurement of odor concentration at the center of the fly bottle ("X" in **A**) during chronic odor exposure over the course of 24 hours. Each trace is the odor profile averaged across 45 consecutive odor pulses (collected over 15 min), sampled every two hours over a 24-hour period.
C) Raster plots of the spiking responses in an example DL5 PN to a 1 s pulse of either solvent (paraffin oil, grey) or E2-hexenal (10^{-7}, black) in consecutive trials spaced 20 seconds apart. Recordings were established from a fly immediately after two days of chronic exposure to E2-hexenal (10^{-7}) as in **A**). Spontaneous (open circles) and stimulus-evoked (filled circles) firing rates are plotted for each trial.
D) Peristimulus time histograms of measurements in **C**) show that the odor environment reliably evokes high levels of PN firing with little adaptation. The average odor-evoked response across all trials is in black. Responses to presentation of solvent are overlaid in grey.

odors at concentrations previously shown to selectively activate a single class of ORNs (Hong and Wilson, 2015; Olsen et al., 2010), in order to facilitate the subsequent analysis of odor responses in postsynaptic PNs receiving direct versus indirect persistent input. An additional criterion was that the odor stimuli drive strong and consistent levels of neural firing in the PNs receiving direct input from the activated ORN class. Photoionization measurements of the odor stimulus in the rearing bottle demonstrated that the stimulus was stable across more than 24 hours (Figure 1B). Odors were pulsed to minimize neural adaptation to the odor, and the interval between odor pulses delivered to the bottle was 20 seconds. Pilot recordings showed that, at this interstimulus interval, the odors reliably activated cognate PNs to saturating or near saturating firing rates over many trials, with little adaptation of the PN response to the odor (Figure 1C-D, and data not shown; see also Figure 2Q). Thus, although the odor stimuli to which we exposed flies were of significantly lower concentration than what has been used in prior studies investigating olfactory plasticity, they drove strong, reliable, and persistent levels of neuronal activity in PNs.

Using these conditions, newly eclosed flies were chronically exposed to E2-hexenal (10^{-7}), which selectively activates ORNs projecting to glomerulus DL5, or solvent (as a control), for two days (see Methods). On day three, we established fluorescently guided, whole-cell current clamp recordings from uniglomerular PNs receiving direct input from the DL5 glomerulus (hereafter referred to as DL5 PNs, Figure 2A), and measured their responses to a concentration series of E2-hexenal. DL5 PNs were identified and targeted for recording based on their expression of GFP, mediated by a genetic driver that specifically labels this cell type (see Methods). DL5 PN responses elicited by moderate to high concentrations of E2-hexenal ($>10^{-8}$) were unchanged in E2-hexenal exposed flies, as compared to controls (Figure 2B, 2Q). However, low concentrations of E2-hexenal (10^{-10} to 10^{-9}) elicited increased levels of odor-evoked membrane depolarization in DL5 PNs from E2-hexenal exposed flies compared to solvent-

exposed flies (Figure 2B). The heightened depolarization of DL5 PNs by weak stimuli corresponded to higher average rates of odor-evoked spiking (Figure 2E).

We quantified these effects by calculating the total depolarization and average evoked firing rate during the first 500 ms after nominal stimulus onset (Figure 2C, 2F). To determine if any differences were arising by chance, we used permutation testing in which we iteratively shuffled the experimental labels of each measurement (E2-hexenal versus solvent exposure) within each stimulus. P-values were calculated directly from the fraction of 10,000 shuffled trials in which the absolute difference between the simulated group means was larger than or equal to the actual observed absolute mean difference (see Figure 2 – figure supplement 1 and Methods). This statistical analysis confirmed that E2-hexenal exposure increased odor-evoked firing rates in DL5 PNs to weak, but not moderate or strong, levels of stimulation (Figure 2F). When firing rates in E2-hexenal exposed flies were normalized to the control rate within each stimulus, we observed an overall increase in odor-evoked DL5 PN firing rate due to E2-hexenal exposure (Figure 2F). Differences in the amount of membrane depolarization between odor- and solvent-exposed groups were not statistically significant at any stimulus concentration (Figure 2C), suggesting a small, but systematic increase in membrane depolarization was nonlinearly amplified by its interaction with the firing threshold in DL5 PNs.

We next examined the extent to which these results generalize to other glomeruli. Using the same approach, we exposed flies to either 2-butanone (10^{-4}), which selectively activates ORNs projecting to glomerulus VM7 (Figure 2G), or geranyl acetate (10^{-4}), which selectively activates ORNs projecting to glomerulus VA6 (Figure 2K). The concentrations of each of these odors was chosen because each selectively and reliably elicits high average firing rates (>100-150 Hz) in the corresponding PN, comparable to the level of E2-hexenal (10^{-7}) activation of DL5 PNs. Again, we chronically exposed flies (separate groups) for two days to each of these stimuli and measured the responses in each PN type (corresponding to the glomerulus receiving direct

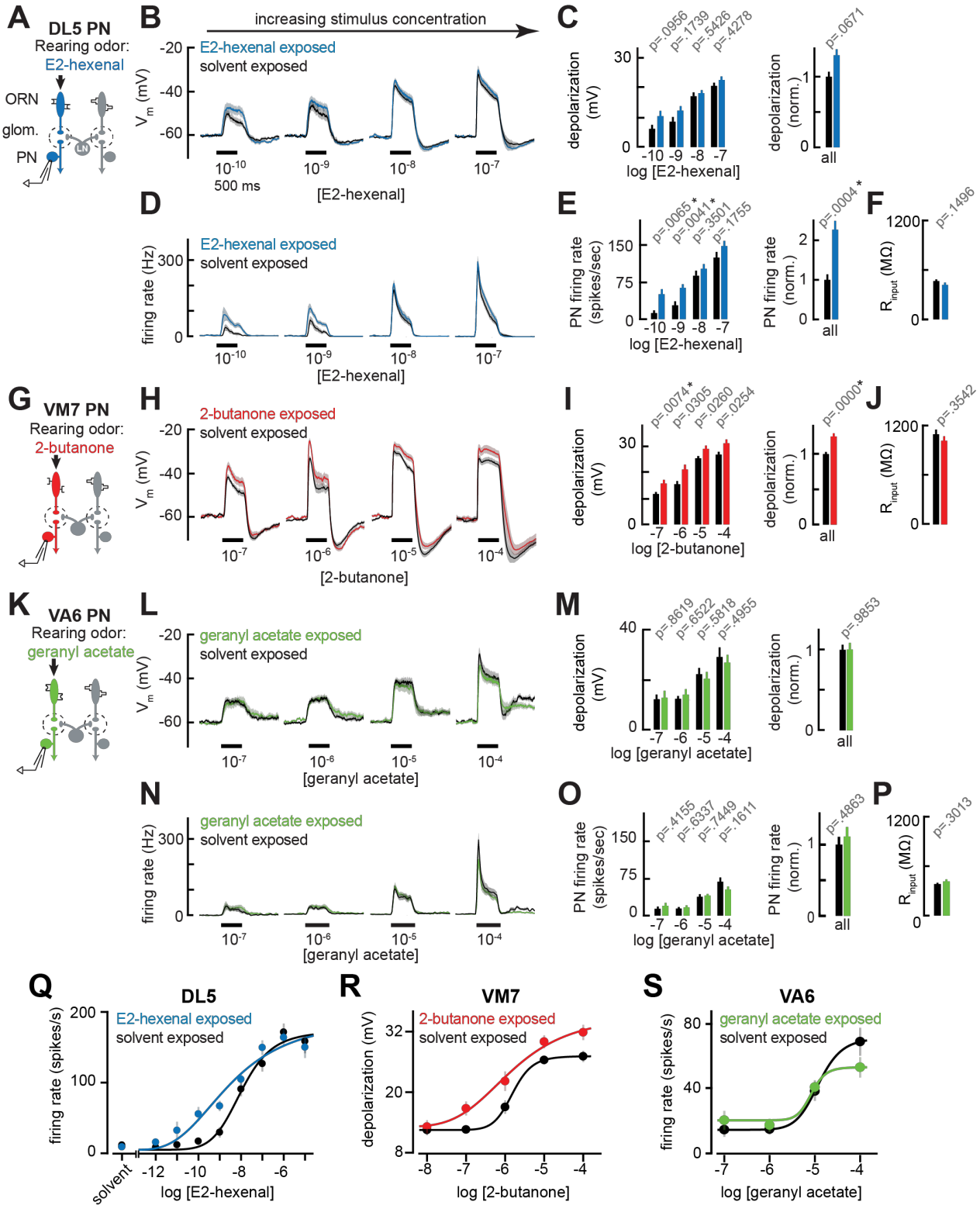

Figure 2: Chronic excitation of direct presynaptic ORN input can modestly enhance PN sensitivity to weak stimuli.
A) Schematic of experimental setup for **B-F**). Recordings were established from DL5 PNs that receive direct presynaptic input from the ORN class (ab4a) chronically activated by the rearing odor (E2-hexenal, 10^{-7}), *n*=7-19 cells.

Figure 2 *(continued)*: B) Odor-evoked depolarization in DL5 PNs in response to varying concentrations of E2-hexenal from flies chronically exposed to E2-hexenal or solvent (paraffin oil).
C) *Left:* Mean odor-evoked depolarization to each stimulus in B) in the 500 ms after nominal stimulus onset. *Right:* Mean normalized odor-evoked depolarization across all stimuli. Within each stimulus, responses were normalized to the mean odor-evoked depolarization in the solvent-exposed group.
D) Peristimulus time histograms of odor-evoked spiking responses in DL5 PNs from B).
E) *Left:* Mean odor-evoked firing rates to each stimulus from D) in the 500 ms after nominal stimulus onset. *Right:* Mean normalized odor-evoked firing rates across all stimuli, computed analogously as in C).
F) Mean input resistance of DL5 PNs recorded from E2-hexenal- or solvent-exposed flies.
G) Experimental setup for **H-J**). Recordings were established from VM7 PNs that receive direct presynaptic input from the ORN class (pb1a) chronically activated by the rearing odor (2-butanone, 10^{-4}), *n*=6-11 cells.
H-I) As in **B-C**) but describing odor-evoked depolarization in VM7 PNs in response to a concentration series of 2-butanone from flies chronically exposed to 2-butanone or solvent.
J) Mean input resistance of VM7 PNs recorded from 2-butanone- or solvent-exposed flies.
K) Experimental setup for **L-P**). Recordings were established from VA6 PNs that receive direct presynaptic input from the ORN class (ab5a) chronically activated by the rearing odor (geranyl acetate, 10^{-4}), *n*=7-11 cells.
L-P) As in **B-F**) but describing odor-evoked responses to varying concentrations of geranyl acetate in VA6 PNs from flies chronically exposed to geranyl acetate or solvent.
Q-S) Response curves in DL5 **(Q)**, VM7 **(R)**, and VA6 **(S)** PNs from odor-exposed and control flies to a concentration series of the cognate odor for each glomerulus. Results from panels **A-P** are replotted here and extended with measurements at additional stimulus concentrations. *n*=3-19 cells.
All plots are mean ± SEM across flies in each experimental condition. One cell was recorded per fly. Two-tailed p-values report the fraction of resampled absolute differences of means (between simulated experimental groups) which are greater than the absolute observed difference between the means of experimental groups (odor-exposed versus solvent-exposed) (see **Methods** and **Figure 2 – figure supplement 1**). Starred (*) *p*-values are significant at the level of α=0.05, corrected for multiple comparisons (Bonferroni adjustment). See Supplemental Table 1 for the full genotype and number of cells in every condition.

Figure 2 – source data 1
Source data for Figure 2B-C, 2D-E, 2H-I, 2L-M, 2N-O.

input from the activated ORNs) to a concentration series of each odor (Figure 2G, 2K). The impact of chronic activation of direct ORN input on odor coding varied in PNs corresponding to different glomeruli. Similar to the DL5 glomerulus, VM7 PNs in 2-butanone-exposed flies exhibited modest increases in odor-evoked depolarization to 2-butanone as compared to control flies, and these effects were more pronounced at weak concentrations (10^{-7}) (Figure 2H-I, 2R). Due to the small size of VM7 PN somata, VM7 PN spikes are small and filtered in comparison to those of other PNs, and odor-evoked spikes riding on large depolarizations could not be reliably counted across all firing rates in our data set. Therefore, for VM7 PNs only, we report odor responses only in terms of membrane depolarization.

In contrast, chronic activation of direct ORN input to VA6 PNs via exposure to geranyl acetate did not alter PN odor responses to the odor across the entire range of concentrations

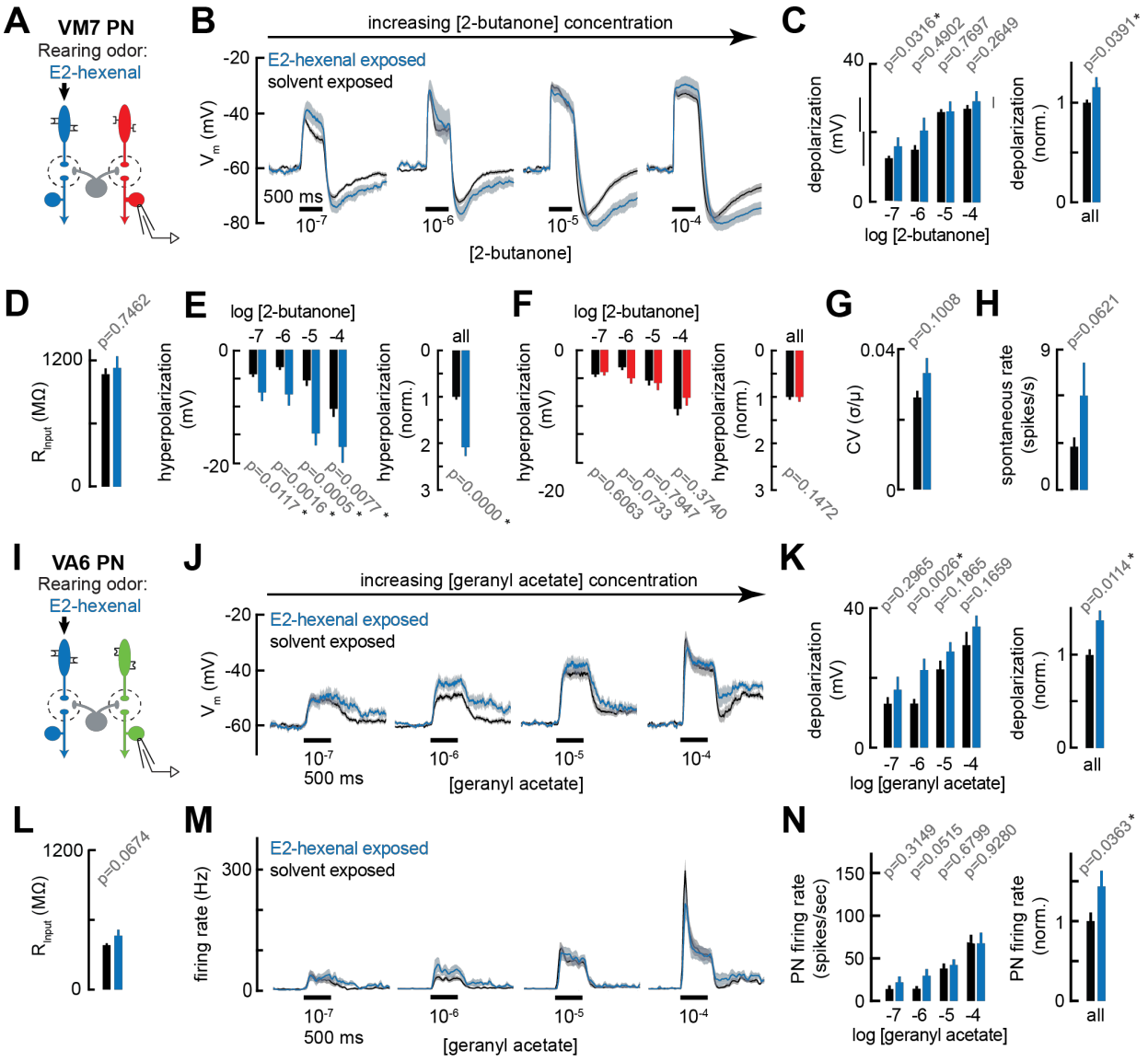

Figure 3: Chronic indirect excitation alters PN response properties.

A) Experimental setup for **B-E**) and **G-H**). Recordings were established from VM7 PNs that receive indirect activity from the ORN class (ab4a) chronically activated by the rearing odor (E2-hexenal, 10^{-7}), *n*=3-11 cells.

B) Odor-evoked depolarization in VM7 PNs in response to varying concentrations of 2-butanone from flies chronically exposed to E2-hexenal or solvent (paraffin oil).

C) *Left:* Mean odor-evoked depolarization to each stimulus from B) in the 500 ms after nominal stimulus onset. *Right:* Mean normalized odor-evoked depolarization across all stimuli. Within each stimulus, responses were normalized to the mean odor-evoked depolarization in the solvent-exposed group.

D) Mean input resistance of VM7 PNs recorded from E2-hexenal- or solvent-exposed flies.

E) *Left:* Mean post-stimulus hyperpolarization in VM7 PN responses to each stimulus from B), calculated over a 2.5 s window after stimulus offset. *Right:* Mean normalized post-stimulus hyperpolarization across all stimuli. Within each stimulus, responses were normalized to the mean post-stimulus hyperpolarization in the solvent-exposed group.

F) Same as **E**), but for VM7 PNs from **Figure 2H** with chronic activation of direct ORN input. Measurements are from VM7 PN recordings in flies chronically exposed to 2-butanone (red) or solvent (black), *n*=6-11 cells.

G) Mean coefficient of variation (CV) of membrane potential in VM7 PNs (from **B**), computed over the 5 s window before stimulus onset, in E2-hexenal- or solvent-exposed flies.

H) Mean spontaneous firing rate of VM7 PNs (from **B**) during the 5 s window before stimulus onset in E2-hexenal- or solvent-exposed flies.

Figure 3 *(continued)*: I) Experimental setup for **J-N**). Recordings were established from VA6 PNs that receive indirect activity from the ORN class (ab4a) chronically activated by the rearing odor (E2-hexenal, 10^{-7}), *n*=5-11.
J-K) As in **B-C**) but for odor-evoked depolarization in VA6 PNs to varying concentrations of geranyl acetate. **L)** As in D) but for VA6 PNs.
M-N) As in **B-C**) but for odor-evoked spiking in VA6 PNs in response to varying concentrations of geranyl acetate (corresponding to J), from flies chronically exposed to E2-hexenal (10^{-7}) or solvent (paraffin oil).
All plots are mean ± SEM across flies, one cell/fly, in each experimental condition. *p*-values are as described in Figure 2. See Supplemental Table 1 for the full genotype and number of flies in every condition.

Figure 3 – source data 1
Source data for Figure 3B-C, 3E-F, 3J-K, 3M-N.

tested, neither at the level of membrane depolarization nor firing rate (Figure 2L-M, 2O-P, 2S). These concentrations elicited levels of membrane depolarization (ranging from 10 to 30 mV) which were similar to that at which other PN types exhibited plasticity after chronic exposure. Together, these results demonstrate that, in some glomeruli like DL5 and VM7, chronic activation of direct ORN input modestly enhanced PN odor responses to weak excitation, resulting in an overall expansion of the range of stimulus concentrations dynamically encoded by PN activity. However, this effect does not appear to be universal across all glomeruli.

Chronic indirect excitation alters PN response properties

Although olfactory input is compartmentalized into feedforward excitatory channels organized around each glomerular unit, odor processing depends on an extensive network of local neurons (LNs) that mediate lateral excitatory and inhibitory interactions among glomeruli (Wilson, 2013). Thus, PN odor responses reflect both direct input, from its presynaptic ORN partners, and indirect input, arising from activity in other glomeruli and received via local lateral circuitry. Having observed that chronic activation of an ORN subtype that provides direct input to a PN can elicit some plasticity in that PN, we next asked whether this plasticity is selective for those PNs directly postsynaptic to the chronically active ORNs, or whether PNs that receive only indirect activity from the chronically active ORN subtype are similarly affected. To address this question, we next evaluated odor responses in VM7 and VA6 PNs from flies chronically exposed to E2-hexenal (10^{-7}) (Figure 3A, 3I), which elicits direct olfactory input to the DL5 glomerulus.

Chronic indirect excitation evoked plasticity with varying properties in different PNs. (Figure 3B-H, 3J-K). In E2-hexenal exposed flies, non-DL5 PNs showed mildly enhanced responses to weak stimuli (Figure 3B, 3D). This effect was small but consistently observed in both VM7 and VA6 PNs at the level of odor-evoked depolarization (Figure 3D, 3K). In VM7 PNs, the baseline spontaneous firing rate was also slightly elevated in E2-hexenal exposed flies as compared to controls (Figure 3G-H). Finally, chronic indirect excitation impacted the post-stimulus response properties of some PNs. For example, odor-evoked depolarization in VM7 PNs from E2-hexenal-exposed flies had a more pronounced and prolonged afterhyperpolarization as compared to controls (Figure 3B, 3E), or as compared to flies that experienced chronic direct excitation (2-butanone exposed) (Figure 2H, 3F). This effect does not appear to generalize to all glomeruli. VA6 PNs, for instance, normally exhibit comparatively different post-stimulus response dynamics, characterized by an epoch of delayed excitation that persists beyond odor offset (Figure 3J). In recordings from VA6 PNs in E2-hexenal exposed flies, this post-stimulus excitation was enhanced across multiple odor concentrations, as compared to solvent-exposed controls (Figure 3J-K). Most of these differences, however, were within the range of subthreshold depolarizations, and so the overall impact of chronic indirect excitation on VA6 firing rates was minimal (Figure 3M-N). Together, these experiments demonstrated that chronic, focal excitation of a single ORN class can lead to changes in PN odor response properties in multiple glomeruli, including in glomeruli not receiving direct synaptic input from the chronically activated ORN class. This result implicates local lateral circuitry in the antennal lobe in odor-experience dependent neural plasticity.

PN coding of odor mixtures is unaffected by chronic odor exposure

So far we have evaluated PN odor responses using atypical odor stimuli, specifically chosen to activate only a single ORN class. We began with this approach so that the presynaptic

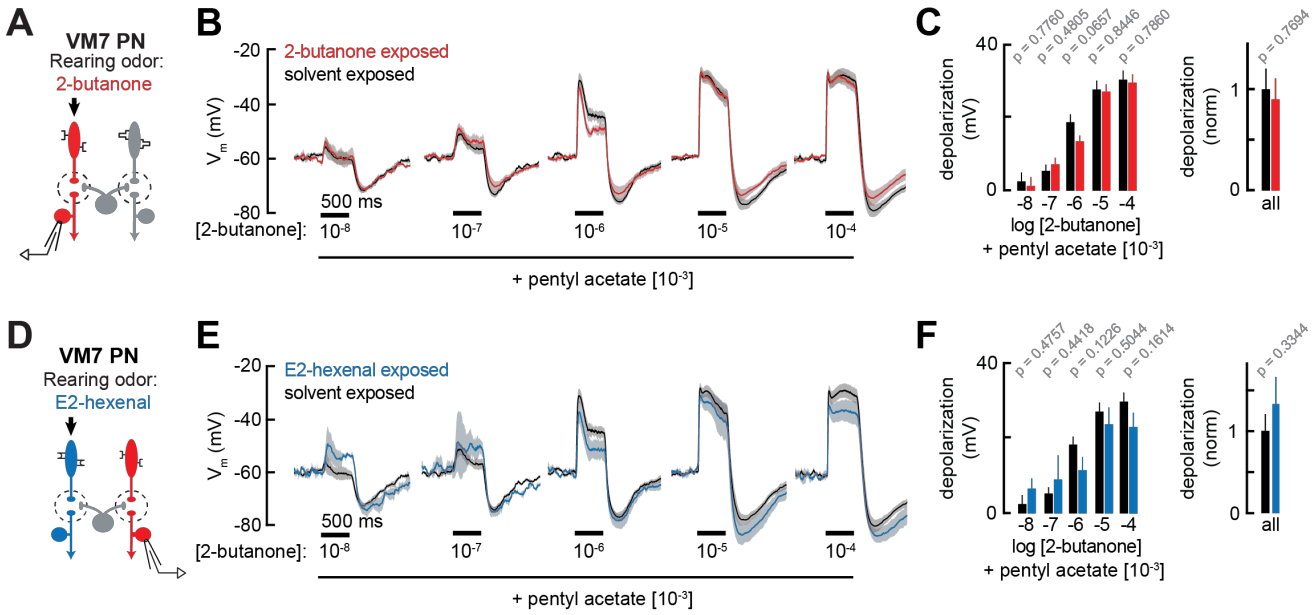

Figure 4: PN responses to odor mixtures are unaffected by chronic activation of direct or indirect ORN inputs.
A) Experimental setup for **B-C)**, which is the same as in Figure **2G-J**. Recordings were established from VM7 PNs that receive direct input from the ORNs (pb1a) chronically activated by the rearing odor (2-butanone, 10^{-4}), *n*=3-7 cells.
B) Odor-evoked depolarization in VM7 PNs from 2-butanone- or solvent-exposed flies to binary mixtures comprised of increasing levels of 2-butanone (10^{-8} through 10^{-4}) blended with a fixed concentration of pentyl acetate (10^{-3}).
C) *Left:* Mean odor-evoked depolarization to each stimulus in B) in the 500 ms after nominal stimulus onset. *Right:* Mean normalized odor-evoked depolarization across all stimuli. Within each stimulus, responses were normalized to the mean odor-evoked depolarization in the solvent-exposed group.
D) Experimental setup for **E-F)**, which is the same as in Figure **3A-E**. Recordings were established from VM7 PNs which receive indirect activity from the ORNs (ab4a) chronically activated by the rearing odor (E2-hexenal, 10^{-7}), *n*=3-7 cells.
E-F) Same as in **B-C**), but for VM7 PNs from E2-hexenal or solvent-exposed flies.
All plots are mean ± SEM across flies (one cell/fly) in each experimental condition. *p*-values are as described in Figure 2. See Supplemental Table 1 for the full genotype and number of flies in every condition.

Figure 4 – source data 1
Source data for Figure 4B-C, 4E-F.

source of odor-evoked input with respect to each PN type was unambiguous; however, typical odors activate multiple ORN classes (de Bruyne et al., 2001; Hallem and Carlson, 2006). Thus, we next investigated how chronic odor exposure impacts the coding of typical odor stimuli that elicit mixed direct and indirect synaptic input to PNs.

As before, we recorded from VM7 PNs in flies chronically exposed to E2-hexenal (10^{-7}), 2-butanone (10^{-4}), or solvent (Figure 4A, D). We mixed a fixed concentration of pentyl acetate (10^{-3}), a broadly activating odor that drives activity in many ORN types (but does not activate pb1a, the VM7 ORN), with increasing concentrations of 2-butanone, the odor that elicits direct activity in VM7 (Nagel and Wilson, 2011; Olsen et al., 2010). Overall, blending pentyl acetate with

2-butanone reduced VM7 PN responses, as compared to their response to 2-butanone alone (Figure 4B, 2H and Figure 4E, 3B). Such mixture inhibition is well understood to be a consequence of lateral GABAergic inhibition elicited by activity in non-VM7 ORNs (Olsen and Wilson, 2008; Olsen et al., 2010). Whereas responses of VM7 PNs to direct excitation (driven by 2-butanone) were modestly enhanced in 2-butanone exposed flies (Figure 2H-I), VM7 responses to mixed direct and indirect input (driven by blends of 2-butanone and pentyl acetate) were similar in control and 2-butanone exposed flies (Figure 4B-C). This effect was observed across a wide range of concentrations of 2-butanone, each blended with a fixed concentration of pentyl acetate. Similar results were observed when we recorded odor mixture responses from VM7 PNs in E2-hexenal exposed flies (Figure 4D), which received chronically elevated indirect activity. Whereas chronic exposure to E2-hexenal altered VM7 PN responses to direct excitation elicited by 2-butanone (Figure 3B-C, 3E), VM7 PN responses to odor mixtures of 2-butanone and pentyl acetate were indistinguishable between E2-hexenal and solvent-exposed flies (Figure 4D-F). These observations suggest that lateral inhibition may also be impacted by chronic odor exposure, such that odor-evoked input elicits more inhibition to counter modest increases in PN excitation. In this way, stable PN responses are maintained to most typical odors which activate many ORs.

When we examined the anatomy of the LN network, however, we observed that it was not grossly affected by chronic odor exposure. Levels of innervation of individual olfactory glomeruli by the neurites of large subpopulations of inhibitory local neurons (iLNs) (measured as the ratio of iLN neurites to total synaptic neuropil) were largely unchanged by chronic odor exposure (Figure 5A-B, F). Unexpectedly, in flies chronically exposed to E2-hexenal only, many glomeruli were smaller in volume than their counterparts in solvent-exposed flies (Figure 5G-I). This trend was observed in most glomeruli measured, including DL5, the glomerulus that receives direct input from E2-hexenal, but was not observed in parallel experiments where flies

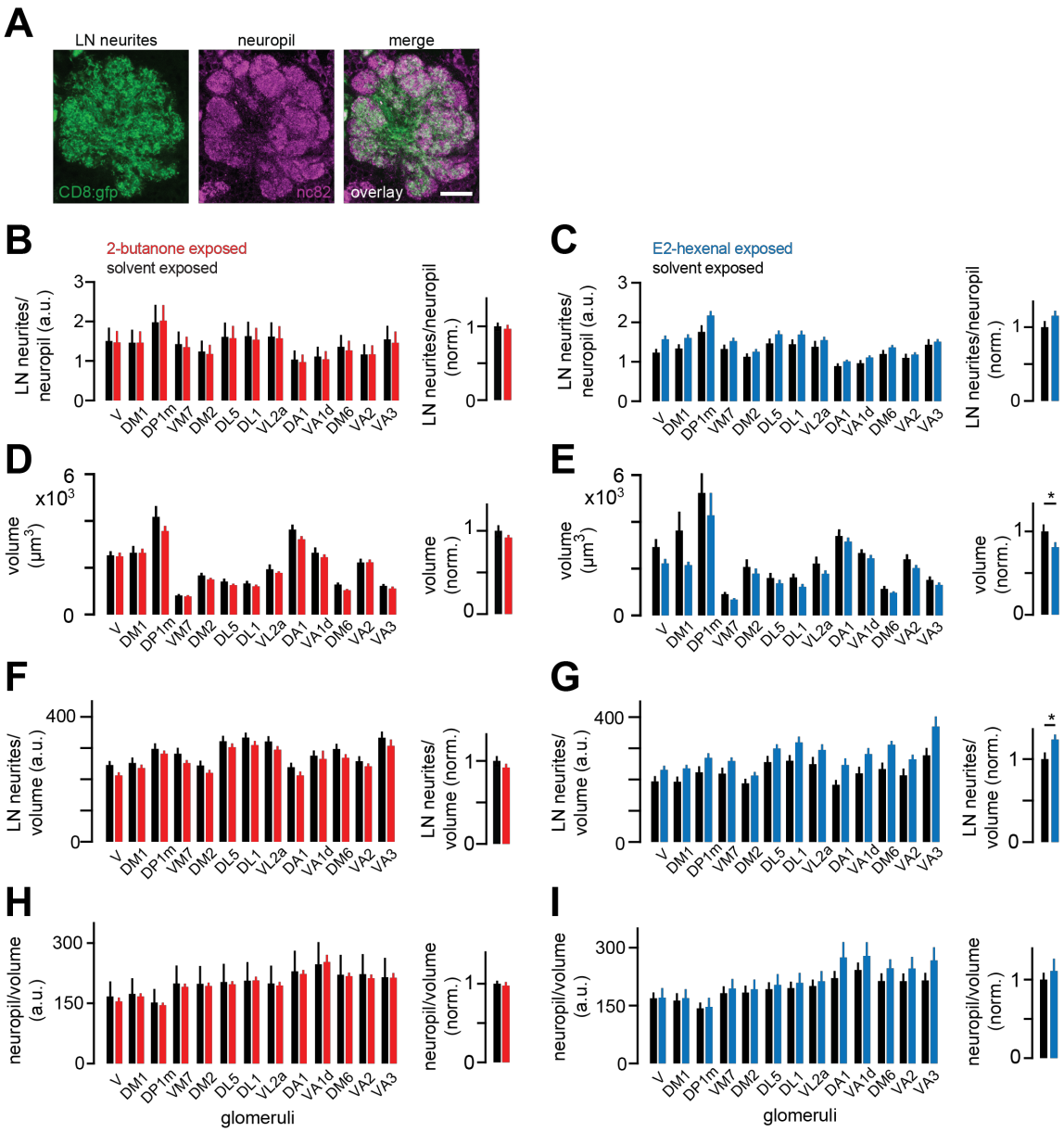

Figure 5: LN innervation of antennal lobe glomeruli is unchanged by chronic excitation of a single ORN class.
A) Single confocal section through the antennal lobe of a fly expressing membrane-targeted GFP (CD8:GFP, green) in a large subset of LNs. Synaptic neuropil was immunostained using the nc82 antibody (magenta) to visualize glomerular boundaries. Scale bar, 20µm.
B-C) *Left:* Ratios of mean LN neurite signal to mean synaptic neuropil signal in each indicated glomerulus in flies chronically exposed to solvent (paraffin oil) versus 2-butanone (10^{-4}) **(B)**, or to solvent (paraffin oil) versus E2-hexenal (10^{-7}) **(C)**. *Right:* Mean normalized ratio of LN neurites to neuropil across glomeruli. Within each glomerulus, values were normalized to the mean ratio of the solvent-exposed group.
D-E) Same as **B-C)** but for the volume of each glomerulus.
F-G) Same as **B-C)** but for the volumetric density of LN neurite signal in each glomerulus.
H-I) Same as **B-C)** but for the volumetric density of synaptic neuropil signal in each glomerulus.
All plots are mean ± SEM across flies in each experimental condition, n=8-13 flies. *p<0.05, two-tailed Mann-Whitney U-test with Bonferroni multiple comparisons adjustment. See Supplemental Table 1 for the full genotype and number of flies in every condition.

Figure 5 – source data 1
Source data for Figure 5B-I.

were chronically exposed to 2-butanone (Figure 5C-E). Thus, chronic exposure to some, but not all, odors can elicit widespread anatomical perturbations in the olfactory circuit. In contrast with previous reports (Das et al., 2011; Devaud et al., 2001; Sachse et al., 2007), however, under our conditions of selective chronic activation, changes in glomerular volume were not odor- or glomerulus- specific, but rather extended globally beyond the chronically active glomerulus.

Chronic activation of ORNs does not alter their odor response properties

Prior studies have suggested that chronic odor exposure increases the sensitivity of ORNs (Chakraborty et al., 2009; Iyengar et al., 2010). We wondered if, in flies chronically exposed to some odors, heightened PN responses to weakly activating input (which elicits little lateral inhibition) might stem directly from changes in ORN activity. Heightened ORN sensitivity might not be apparent in PN responses to stronger odors in odor-exposed flies if circuit mechanisms such as lateral inhibition, which grow with stimulus strength, were acting to compensate changes in feedforward excitation.

To evaluate how chronic odor exposure affects ORN sensitivity, we exposed flies to E2-hexenal (10^{-7}) or 2-butanone (10^{-4}) as before and recorded extracellular spikes from the ORN classes selectively activated by each odor stimulus (Figure 6A, 6D; see Methods). We observed that chronic activation of either ORN type – ab4a ORNs in E2-hexenal exposed flies or pb1a ORNs in 2-butanone exposed flies – did not significantly impact spontaneous (Figure 6 – figure supplement 1E-G) or odor-evoked firing rates across a wide range of stimulus concentrations (Figure 6B-C, 6E-F, Figure 6 – figure supplement 1A-B), including those lower concentrations which elicited enhanced responses in postsynaptic DL5 or VM7 PNs (Figure 2B-E, 2H-I). In addition, we evaluated pb1a ORN (presynaptic to VM7) responses in E2-hexenal exposed flies (Figure 6G) because VM7 PN responses to odor were enhanced in this condition compared to

controls (Figure 3B-C). These experiments showed that pb1a odor responses were largely unaffected by E2-hexenal exposure (Figure 6H-I). Although we observed a small decrease in response to 2-butanone at a concentration of 10^{-4}, this difference did not consistently trend at nearby concentrations (10^{-5} or 10^{-3}) and did not reach statistical significance after correction for multiple comparisons (Figure 6- figure supplement 1C).

We next considered the possibility that small changes in ORN firing rate might not be resolvable in extracellular recordings from individual neurons, but that the high convergence of ORNs onto PNs could amplify small differences in ORN firing into a measurable increase in PN response. Therefore, we used functional imaging to measure the population response of all ab4a ORNs in the DL5 glomerulus (Figure 6J-K), where the axon terminals of dozens of ab4a ORNs (Grabe et al., 2016) converge in a small physical volume (~200 μm^3). We expressed the genetically encoded calcium indicator GCaMP6f in ab4a ORNs under the control of the Or7a-Gal4 promoter. We then chronically exposed these flies to either E2-hexenal or solvent and used two-photon microscopy to record odor-evoked ORN calcium signals in the DL5 glomerulus (Figure 6K). We found that population imaging of ORN terminals had comparatively higher sensitivity for detecting odor responses, demonstrated by the ability to resolve odor-evoked activity in ab4a ORNs in response to E2-hexenal at a concentration of 10^{-10} (Figure 6L-M), responses which are not detectable by extracellular recordings from individual ORNs (Figure 6B-C). However, functional imaging showed that odor-evoked responses in ab4a ORN terminals in glomerulus DL5 were indistinguishable between E2-hexenal exposed and control flies across the entire range of odor concentrations tested (Figure 6L-M, Figure 6- figure supplement 1D). Taken together, these results indicate that ORN odor responses are unaffected by perturbations in the odor environment that drive over a million additional spikes in each ORN over the course of two days of exposure. They also imply that the PN plasticity we observe likely stems from central cellular or circuit mechanisms, rather than from changes at the periphery.

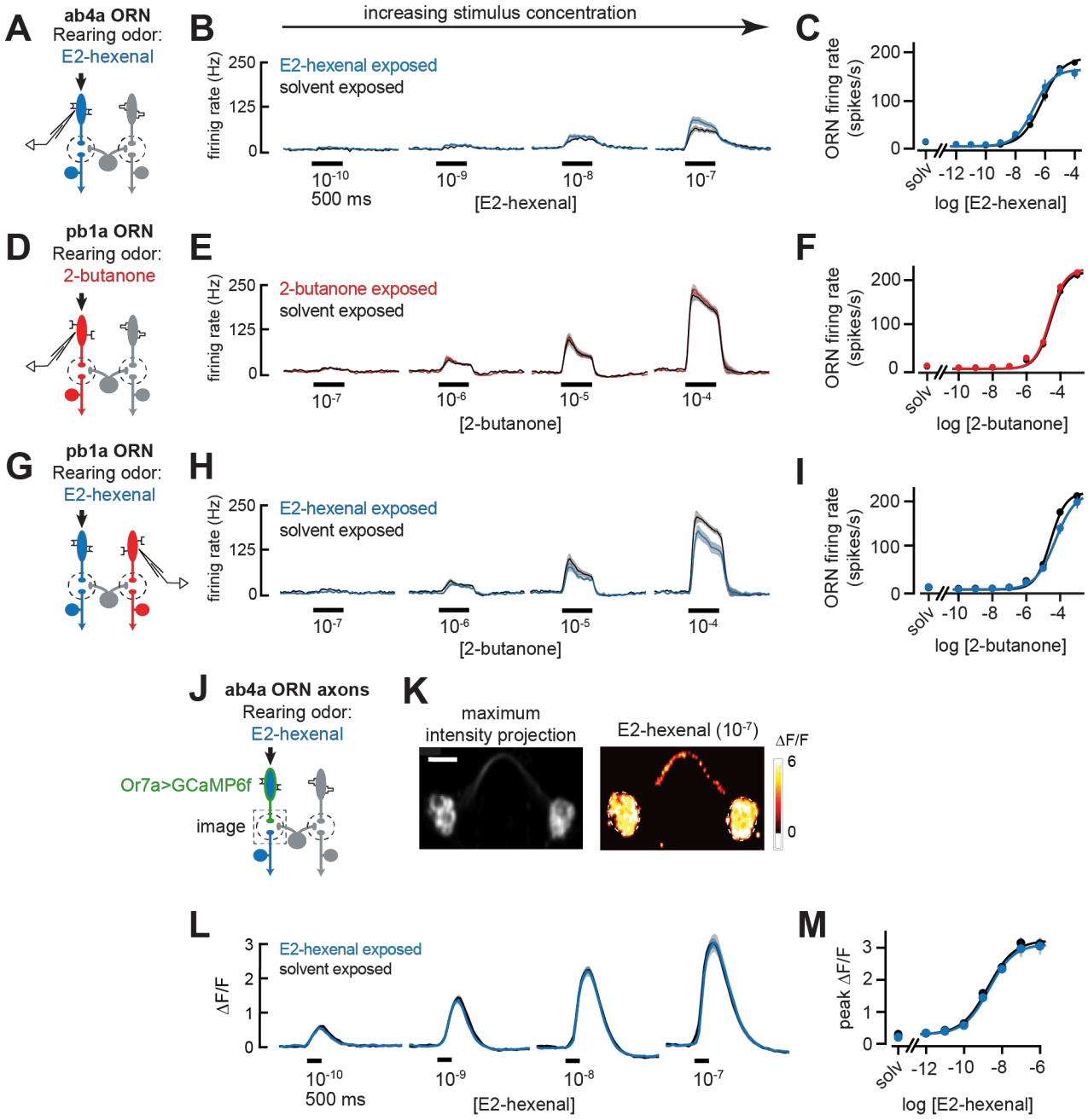

Figure 6: Odor responses in ORNs are unaffected by chronic odor exposure.

A) Experimental setup for **B-C)**. Single-sensillum recordings (SSR) were established from ab4a ORNs, which are directly excited by the rearing odor E2-hexenal (10^{-7}), *n*=6-12 cells.

B) Peristimulus time histograms of odor-evoked spiking in ab4a ORNs in response to varying concentrations of E2-hexenal from flies chronically exposed to E2-hexenal or solvent (paraffin oil).

C) Response curve of mean baseline-subtracted ab4a firing rates (calculated over the 500 ms window of stimulus presentation) to varying concentrations of E2-hexenal in E2-hexenal- or solvent-exposed flies. The concentration-response curve includes responses from **B)**, as well as measurements at additional stimulus concentrations. solv, solvent (paraffin oil).

D) Experimental setup for **E-F)**. SSR recordings from pb1a ORNs, which are directly excited by the rearing odor 2-butanone (10^{-7}), *n*=6-11 cells.

E-F) Same as **B-C)**, but for pb1a ORNs responding to varying concentrations of 2-butanone in flies chronically exposed to 2-butanone or solvent.

Figure 6 *(continued)*: G) Experimental setup for **H-I)**. SSR recordings from pb1a ORNs in flies chronically exposed to E2-hexenal (10^{-7}), a stimulus which directly excites ab4a ORNs, *n*=5-11 cells.
H-I) Same as **B-C)**, but for pb1a ORNs responding to varying concentrations of 2-butanone in flies chronically exposed to E2-hexenal or solvent.
J) Experimental setup for **K-M)**. GCaMP6f was expressed in ab4a ORNs under the control of *or7a-gal4*. Flies were chronically exposed to E2-hexenal (10^{-7}) or solvent, and odor-evoked calcium responses in ab4a ORN terminals were imaged in the DL5 glomerulus (dashed box) using two-photon microscopy, *n*=6-8 cells.
K) *Left:* Maximum intensity projection of the imaging plane across the time series of an example stimulus presentation. *Right*: Peak ΔF/F heat map from a single experiment evoked by a 500 ms pulse of E2-hexenal (10^{-7}) in a solvent-exposed fly, averaged across three stimulus presentations. Scale bar is 5 μm.
L) Time courses of change in fluorescence in ab4a ORN terminals elicited by varying concentrations of E2-hexenal in E2-hexenal- and solvent-exposed flies.
M) Response curve of mean peak ΔF/F responses to varying concentrations of E2-hexenal in E2-hexenal- or solvent-exposed flies. The concentration-response curve includes responses from L), as well as measurements at additional stimulus concentrations. solv, solvent.
All plots are mean ± SEM across flies in each experimental condition (one cell or antennal lobe/fly). Statistical analysis was as in Figure 2 (see **Figure 6 – figure supplement 1** for p-values); none of the comparisons in **Figure 6** between odor- and solvent-exposed groups are statistically significant at the α=0.05 level, with Bonferroni adjustment for multiple comparisons. See Supplemental Table 1 for the full genotype and number of flies in every condition.

Figure 6 – source data 1
Source data for Figure 6B-C, 6E-F, 6H-I, 6L-M.

The role of central circuit mechanisms in olfactory plasticity

We next investigated several central mechanisms that might contribute to olfactory plasticity. First, we asked whether chronic odor exposure changes the intrinsic cellular excitability of PNs. Comparisons of the input resistance of PNs recorded in odor-exposed and control flies showed that postsynaptic input resistance was unaltered by chronic exposure to any of the odors in our study, regardless of whether PNs received direct or indirect chronic activation (Figures 2F, 2J, 2P, 3D, 3L). Consistent with these observations, *f-I* curves directly measuring the firing rate of deafferented DL5 PNs in response to current injection at the soma (Figure 7A) were indistinguishable between control and E2-hexenal exposed flies (Figure 7B-C; see also Figure 7 – figure supplement 1A-B). These results indicate that the intrinsic excitability of PNs is unaltered by chronic odor exposure and does not account for the increase in PN sensitivity to weak odors.

Next, we asked whether ORN-PN synaptic strength is impacted by chronic odor exposure. In each glomerulus, many axon terminals from the same ORN class synapse onto each uniglomerular PN, and each ORN communicates with each PN via multiple active zones

(Horne et al., 2018; Kazama and Wilson, 2008; Rybak et al., 2016; Tobin et al., 2017). We refer to the combined action of all the neurotransmitter release sites between a single ORN and a PN as a unitary ORN-PN synapse. To measure the strength of a unitary synaptic connection between ab4a ORNs and DL5 PNs, we adapted a previously established minimal stimulation protocol (Kazama and Wilson, 2008) for use with optogenetic-based recruitment ORN activity. We expressed the channelrhodopsin variant Chrimson (Klapoetke et al., 2014) in all ab4a ORNs, driven from the Or7a promoter (Couto et al., 2005), acutely severed the antennal nerve, and stimulated ORN terminals with wide-field light delivered through the imaging objective. Concurrently, we monitored synaptic responses in DL5 PNs using targeted whole-cell recordings in voltage clamp mode (Figure 7D).

We employed a minimal stimulation protocol to isolate unitary excitatory postsynaptic currents (uEPSCs) evoked by single presynaptic ORN spikes. Stimulation with very low levels of light elicited no synaptic response in the PN (Figure 7E). As the power density was gradually increased, trials of mostly failures were interspersed with the abrupt appearance of an EPSC in an all-or-none manner. Further ramping the light in small increments had no effect on the amplitude of the EPSC in the PN, until a power density was reached where the EPSC amplitude abruptly doubled, as compared to the amplitude of the initially recruited EPSC (Figure 7E). Light-evoked EPSCs were dependent on providing flies with the rhodopsin chromophore all-trans-retinal (ATR) in their food; PNs from flies raised on non-ATR supplemented food displayed no light-evoked responses (data not shown). The step-like profile of EPSC amplitudes as a function of power density likely reflects the discrete recruitment of individual ORN axon fibers with increasing stimulation. In particular, the sharp transition from mostly failures to a reliably evoked current is consistent with the response arising from the activation of a single ORN input. The time from the onset of light stimulation to the evoked uEPSC was variable and averaged approximately ~23 ms $\pm$ 2.2 ms (s.d.) (Figure 7- figure supplement 1C), similar to the distribution

of latencies to the first light-evoked ORN spike at comparable intensities (data not shown; (Jeanne and Wilson, 2015)). Using this optogenetic-based ORN recruitment method, the amplitude (~40 pA), rise time (~2 ms), and half decay time ($t_{1/2}$ ~ 7ms) of uEPSCs in DL5 PNs

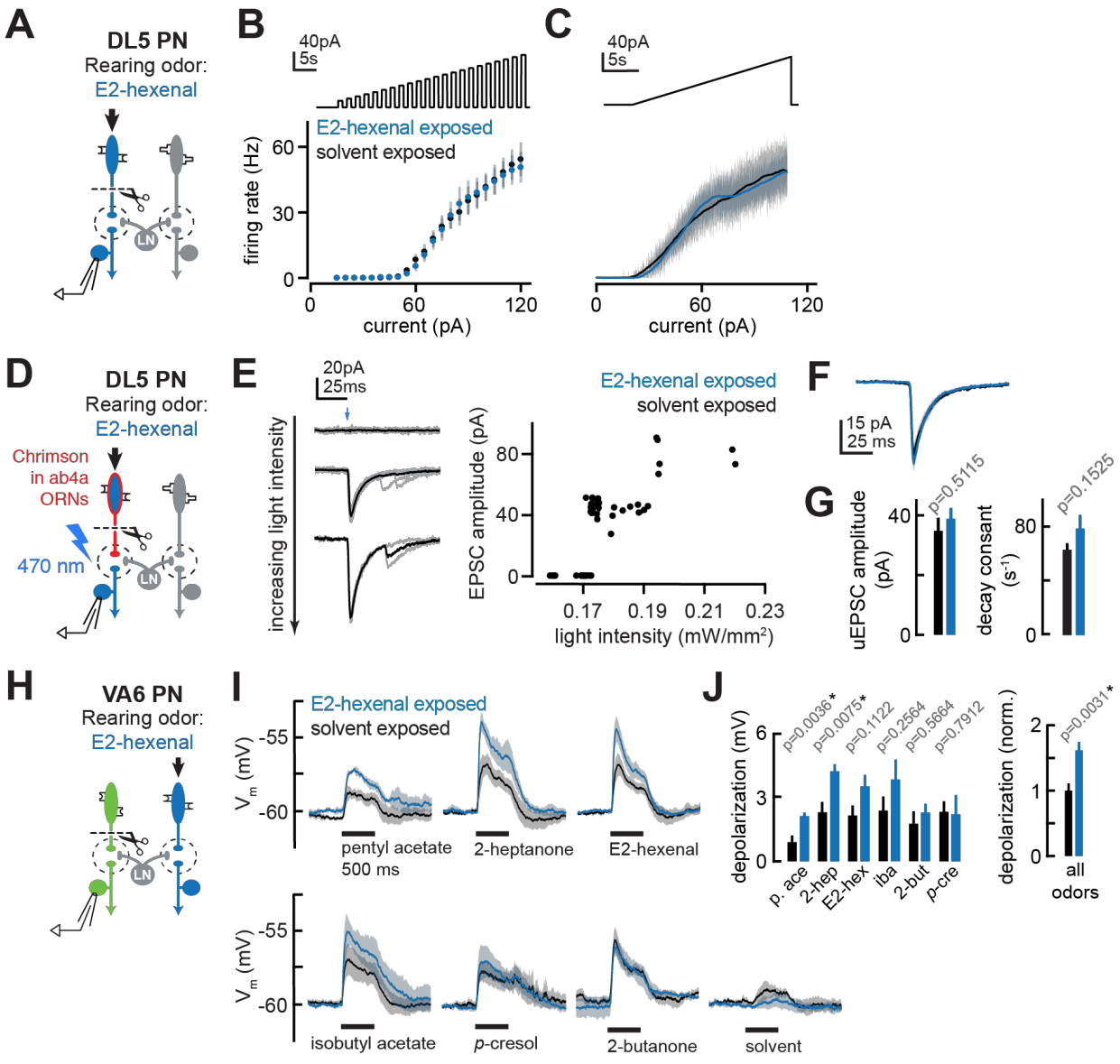

Figure 7: The effect of chronic ORN activation on PN intrinsic properties, ORN-PN synapse strength, and lateral excitation in the antennal lobe.

A) Experimental setup for **B-C)**. Recordings were established from DL5 PNs, which receive direct presynaptic input from the ORN class (ab4a) chronically activated by the rearing odor (E2-hexenal, 10^{-7}), *n*=4 cells. Immediately prior to recording, PNs were deafferented by bilateral transection of the antennal nerves.

B) *f-I* curve of DL5 PNs from E2-hexenal- and solvent-reared flies plotting firing rates elicited by increasing levels of current injection (1 s pulses delivered at an interpulse interval of 1 s and increasing with a step size of 5 pA).

C) Same as **B)** but plotting firing rates elicited by injection of a slow triangular current ramp (4.5 pA/s). Firing rate was calculated in 50ms bins with 25ms overlap.

D) Experimental setup for measurement of synaptic strength between ab4a ORNs and DL5 PNs in **E-G)**. Flies expressing the channelrhodopsin CsCrimson in ab4a ORNs under the control of *or7a-gal4* were chronically exposed to E2-hexenal (10^{-7}) or solvent. Immediately prior to the experiment, PNs were deafferented by bilateral transection of the antennal nerves. Recordings were established from DL5 PNs, and unitary EPSCs were elicited in PNs by light-based minimal stimulation of presynaptic ORN terminals. *n*=5-7 cells.
E) A minimal stimulation protocol recruits unitary EPSCs. *Left*: EPSCs recorded in a DL5 PN (from a solvent-exposed fly) in response to increasing levels of light-based (488 nm) ORN stimulation (blue arrow). Individual trials are in grey; the average of all trials at a given light intensity is in black. *Right*: EPSC amplitude as a function of light intensity. Each dot represents the peak EPSC amplitude from a single trial. As light intensity is gradually increased, an evoked EPSC
Figure 7 *(continued)*: appears abruptly, and its amplitude remains constant as the light intensity is further increased. This range (~0.17-0.19 mW/mm^2) likely corresponds to recruitment of an action potential in a single ab4a ORN axon presynaptic to the DL5 PN. As the level of light driven ORN stimulation further increases, the amplitude of the evoked EPSC suddenly doubles, likely reflecting the recruitment of a second axon.
F) Mean unitary EPSC recorded in DL5 PNs from E2-hexenal- or solvent-exposed flies.
G) Mean unitary EPSC amplitude (left) and decay rate (right) in DL5 PNs from E2-hexenal- or solvent-exposed flies.
H) Experimental setup for **I-J)**. Recordings were established from VA6 PNs in flies chronically exposed to E2-hexenal or solvent. Immediately prior to recording, PNs were deafferented by bilateral transection of the antennal nerves. Odors stimulate intact ORNs located in the palps and recruit lateral input to VA6 PNs (which normally receive direct input from ORNs in the antenna). *n*=3-5 cells.
I) Odor-evoked depolarization in deafferented VA6 PNs elicited by the indicated stimuli in flies chronically exposed to E2-hexenal or solvent (paraffin oil). Odors were presented at 10^{-2} dilution.
J) *Left:* Mean odor-evoked depolarization to each stimulus in **I)** in the 500 ms after nominal stimulus onset. *Right:* Mean normalized odor-evoked depolarization across all stimuli. Within each stimulus, responses were normalized to the mean odor-evoked depolarization in the solvent-exposed group.
All plots are mean ± SEM across flies in each experimental condition (one cell/fly). *p*-values are as described in **Figure 2**. See Supplemental Table 1 for the full genotype and number of flies in every condition.

Figure 7 – source data 1
Source data for Figure 7B-C, 7F-G, 7I-J.

(Figure 7F) in the control condition were similar to previous measurements made using conventional electrical stimulation of the antennal nerve (Kazama and Wilson, 2008), confirming this method for measuring unitary ORN-PN synapse properties.

We used this method to record uEPSCs from DL5 PNs in flies chronically exposed to either solvent or E2-hexenal (10^{-7}), the odor which directly activates the presynaptic ORNs. In order to compare recordings across different trials, individual uEPSCs from each condition were aligned by their peaks and averaged. Average DL5 uEPSC amplitudes and response kinetics were indistinguishable between solvent and E2-hexenal exposed flies (Figure 7F-G). This result shows that ORN-PN strength is unchanged by chronic odor exposure and is unlikely to account for enhanced DL5 PN responses to weak stimuli in E2-hexenal exposed flies.

Finally, we considered the possibility that local lateral excitatory connections play a role in PN plasticity triggered by chronic odor exposure. Olfactory glomeruli in the antennal lobe are densely interconnected by a network of lateral excitatory local neurons (eLNs) that signal globally

via electrical synapses to boost PN excitability (Olsen et al., 2007; Root et al., 2007; Shang et al., 2007; Yaksi and Wilson, 2010). The effects of lateral excitation on PN responses are most significant in the regime of weak odor stimuli (Shang et al., 2007; Yaksi and Wilson, 2010). Lateral excitatory input to PNs is most directly measured by removing the source of direct input to the PN and recording PN activity while stimulating ORNs that directly excite other glomeruli (Olsen et al., 2007; Root et al., 2007; Shang et al., 2007). The fly has two sets of olfactory organs – the antennae and the palps – and each ORN class resides in one or the other, but never both. We chronically exposed files to either solvent or E2-hexenal (10^{-7}), bilaterally removed the antennae, and established recordings from VA6 PNs while stimulating the palps with odor (Figure 7H). Since VA6 PNs receive direct input from ORNs located in the antenna, VA6 PN odor responses recorded in this configuration stem from lateral (indirect) input that originates from ORNs located in the palp.

The stimulus panel for this experiment was comprised of odors that broadly activate many ORN classes, including those housed in the palps. As previously shown (Olsen et al., 2007; Yaksi and Wilson, 2010), different odors elicit differing, but characteristic amounts of lateral excitation in VA6 PNs (Figure 7I). Many, but not all, odors evoked increased lateral excitation in VA6 PNs from E2-hexenal exposed flies, as compared to solvent-exposed flies (Figure 7I-J). To pool our measurements of lateral excitatory responses in VA6 PNs across stimuli, we normalized the amount of PN membrane depolarization elicited by each odor in E2-hexenal exposed flies to the average amount it elicited in solvent-exposed flies. This analysis confirmed that the average amount of odor-evoked lateral excitation across all stimuli was increased in E2-hexenal exposed flies, as compared to solvent-exposed controls (Figure 7J). These results suggest that chronic odor exposure increases the overall strength of global excitatory coupling among glomeruli in the antennal lobe after chronic odor exposure, which may contribute to the heightened sensitivity of PNs to weak odors.

DISCUSSION

We find that strong, chronic activation of a single class of olfactory receptor neurons triggers limited plasticity at early stages of olfactory processing in *Drosophila*. Persistent exposure to a monomolecular odorant, delivered to the environment at concentrations that could be realistically encountered in the natural world, elicited mild increases in the olfactory sensitivity of some PNs. This plasticity (when present) affects the responses of PNs to relatively weak odor stimuli, so as to expand the lower range of stimulus intensities dynamically encoded by the PN. Many elements of the antennal lobe circuit, including ORN sensitivity and ORN-PN synapse strength, were unaffected by chronic ORN activation. Plasticity triggered by chronic ORN activity was observed not only in PNs corresponding to the glomerulus that receives direct input from the chronically active ORNs, but also in PNs corresponding to other glomeruli that receive only indirect chronic activity. This result suggests that local neurons, which mediate lateral interactions between glomeruli, participate in olfactory plasticity, consistent with our observation that odor exposure can boost the level of lateral excitatory coupling between some PNs. These results highlight the overall stability of the representation of odors in the antennal lobe, even in odor environments that elicit unusually high levels of activity in a single ORN class, and do not support the hypothesis that ORN and PN olfactory codes adjust to the frequency with which specific odors are encountered in the environment.

Chronic exposure to odors at naturally occurring concentrations elicits limited plasticity in the fly antennal lobe

Chronic activation of at least two ORN classes elicited modest increases in the odor sensitivity of the cognate PNs (DL5 and VM7) receiving direct presynaptic input from each,

417 although a third PN type (VA6) was unaffected (Figure 2). These results contrast with prior studies
418 in fly in which chronic exposure to either carbon dioxide (5% in air) or ethyl butyrate (from a 20%
419 v/v source) resulted in reduced odor responses in PNs that receive direct input from persistently
420 activated ORNs (Das et al., 2011; Sachse et al., 2007). These studies concluded that olfactory
421 plasticity homeostatically adjusts antennal lobe function to maintain the output from each PN
422 type within a desired target range of activity. However, a more recent study observed the
423 opposite, finding that chronic activation of VA6 ORNs mildly enhanced VA6 PN odor responses
424 (Kidd and Lieber, 2016; Kidd et al., 2015). Prior studies in rodents also observed that chronic
425 odor exposure enhances olfactory sensitivity (Cadiou et al., 2014; Liu and Urban, 2017; Wang et
426 al., 1993). Establishing the direction of olfactory plasticity evoked in response to elevated levels
427 of sensory input seems important, as it would point towards differing functional consequences
428 of plasticity for olfactory coding. Methodological differences may contribute to the divergent
429 findings; for instance, in flies, different studies vary with respect to the odor concentration and
430 procedure used for chronic exposure (see below) and the methods used for measuring PN odor
431 sensitivity (calcium imaging versus intracellular electrophysiology). Another possibility is that the
432 rules for plasticity vary depending on the intensity of odor exposure and/or the specific olfactory
433 channel being chronically activated, such that PN sensitivity is adjusted according to specific
434 rules useful for each individual odor and glomerulus. Yet another possibility is that olfactory
435 plasticity is relatively weak in this circuit, and the small magnitude of its effects make it difficult
436 to measure experimentally with high confidence.

437 One of the most significant ways in which our experiments differ from prior work is the
438 structure of the odor environment to which flies are exposed. We exposed flies to periodic one-
439 second pulses of odor at estimated concentrations of ~10 ppb to ~10 ppm in air (see Methods).
440 We confirmed that these stimuli reliably elicited near saturating levels of firing in the targeted PN
441 class every twenty seconds over the course of many hours (Figure 1C-D and data not shown).

This odor exposure paradigm more than doubled the average firing rate of the targeted PN and elicited more than a million extra spikes in the activated PN over the course of the two-day period of exposure (see Methods). We note that, even though the overrepresented odor narrowly activates a single olfactory channel, it was delivered to flies living in an active culture containing cornmeal food, yeast, and other flies. As such, the olfactory circuit is expected to be broadly active during the period of chronic odor exposure. Our goal with this experimental design was to drive a robust change in neural activity in a single ORN type, while still maintaining animals in an olfactory environment that could be plausibly encountered in the natural world. This scenario allowed us to test the hypothesis that olfactory codes can adapt to the statistical frequency with which specific odors are encountered in natural environments, in ways that depend on the relative levels of neural activity in sensory neurons that are sensitive to these stimuli (Barlow, 1961; Fiser et al., 2010).

Nearly all prior studies investigating olfactory plasticity, in flies or mice, use odor exposure paradigms that differ from this study in two ways: first, they continuously expose animals to odor from a stationary source in the home cage; and second, they provide the odor at significantly higher concentrations generally ranging from ~10^3 to ~10^5 ppm in air (Chodankar et al., 2020; Das et al., 2011; Devaud et al., 2001; Liu and Urban, 2017; Sachse et al., 2007; Wang et al., 1993). Such stimuli that are unlikely to be found in natural odor sources; for comparison, headspace concentrations of the most abundant small ester, alcohol, and aldehyde volatiles common in fruit odor sources typically ranges from ~1 ppb to ~10 ppm in air (for instance, Boschetti et al., 1999; Farneti et al., 2017; Jordán et al., 2001). For many such volatiles, prolonged exposure at concentrations that exceed ~10^3 ppm is considered hazardous to human life or health (NIOSH, (2019)). The impact of prolonged exposure to very intense odors on the olfactory circuit should be interpreted in the context of the likelihood of encountering such stimuli during the natural evolutionary history of the fly.

Our study is also distinct in that we characterized how the odor exposure environment impacts olfactory neuron firing rates, motivated by a desire to understand how manipulation of PN firing rates relates to changes in circuit function. In preliminary experiments where we continually exposed flies to a constant pulse of odor, PN firing rates adapted strongly within thirty seconds of stimulus onset to ~20-30% of peak values (data not shown, (Cafaro, 2016; Martelli and Fiala, 2019). This observation motivated our decision to pulse the odor during the exposure period (Figure 1A). In an animal housed with a stationary odor source in the environment, as is common in prior work (Chodankar et al., 2020; Das et al., 2011; Devaud et al., 2001; Liu and Urban, 2017; Wang et al., 1993), increases in olfactory neuron firing rates will be affected by neural adaptation and may depend in complex ways on the animal's movement around objects in the physical environment.

The odor exposure environment used in this study may simply have elicited insufficient levels of neural activity in olfactory neurons to trigger more dramatic levels of plasticity; however, it may also be that olfactory plasticity triggered by very intense odor stimuli needs to be interpreted with caution. Saturating levels of firing in projections neurons are elicited by stimuli many orders of magnitude less intense than odors at ~10^3 to 10^5 ppm; thus, it may not necessarily be the case that anatomical and functional changes induced by exposure to intense odors are mediated only by neural activity-driven processes. Alternatively, direct action of the odor on molecular targets in the fly are formally possible. We note that, even though it was not the focus of this study, understanding how exposure to very intense odors impacts neural function is an important problem, regardless of the mechanism, since both animals and humans frequently encounter such situations in modern industrialized environments (Steinemann, 2016; Wolkoff and Nielsen, 2017; Wypych, 2017).

Stimulus-selective versus global plasticity in sensory circuits

Another important point of divergence between our results and some prior work is that the mild olfactory plasticity we observed was not specific only for the glomerulus receiving direct input from the chronically activated ORN class. Some prior studies showed that the effects of chronic odor exposure on olfactory neuron responses and anatomical volume were selective for specific glomeruli, although the direction of these effects varied between studies (Chakraborty et al., 2009; Das et al., 2011; Devaud et al., 2001, 2003; Sachse et al., 2007). Most studies chronically exposed flies to odors that broadly activate many ORN classes, complicating the interpretation of the degree of selectivity of olfactory plasticity. However, Sachse et al. also used an experimental design that chronically activated a single ORN class, the ab1C ORNs projecting to glomerulus V), and found that plasticity selectively affected PNs in glomerulus V (Sachse et al., 2007). Determining the degree to which olfactory plasticity is stimulus- and glomerulus-specific is significant because it has implications for whether olfactory plasticity can reshape the olfactory code to reflect recent stimulus statistics in the environment. Our results, however, indicate that chronic ORN activity triggers mild increases in odor responses in both PNs receiving direct presynaptic input, and PNs receiving indirect input, from the chronically active ORN class. Additionally, we observed that, at least for some odors, chronic ORN activation elicited broad anatomical changes in the olfactory circuit, where all glomeruli, including the glomerulus receiving chronic direct activation, were slightly smaller than their counterparts in control flies (Figure 5E). The effect was observed in flies chronically exposed to E2-hexenal (10^{-7}) but not to 2-butanone (10^{-4}).

Plasticity elicited by chronic indirect input did not impact all PNs equivalently. For example, chronic elevation of indirect input to VM7 PNs (by exposure to E2-hexenal) mildly increased VM7 PN sensitivity and also significantly increased levels of post-stimulus hyperpolarization in the cell. However, this latter effect was not observed in VA6 PNs, which showed only mild increases in activity in response to weak odors and exhibited normal post-

517 stimulus dynamics (Figure 3B, 3J). These results suggest that olfactory plasticity differentially
518 impacts PNs in different glomeruli, possibly due to how the mechanisms underlying plasticity
519 interact with differing intrinsic biophysical characteristics of each PN type.

520 Our observation that chronic odor exposure elicits changes broadly in many PN types is
521 similar to that of a recent functional imaging study in mouse which found that chronic odor
522 exposure in early postnatal life induced widespread, global enhancement of mitral cell excitability
523 across the olfactory bulb (Liu and Urban, 2017). The observation that olfactory plasticity can
524 globally impact odor responses across multiple glomeruli suggests that chronic, persistent ORN
525 activation may function to adjust the overall gain or sensitivity of the circuit, especially in the low
526 contrast stimulus regime. Such a widespread increase in excitability might reflect a form of
527 generalized sensory enrichment that has been previously described in mammalian olfactory
528 (Mandairon et al., 2006b; Rochefort et al., 2002), visual (Beaulieu and Cynader, 1990a, 1990b),
529 and auditory (Engineer et al., 2004) systems .

530

531 **Mechanisms of olfactory plasticity in the antennal lobe**

532 PN odor responses depend on the nonlinear integration of a complex set of inputs, which
533 include feedforward excitation from ORNs, lateral excitation from cholinergic local neurons
534 (eLNs) and lateral inhibition from GABAergic local neurons (iLNs) (Wilson, 2013). In the antennal
535 lobe, the strength of each of these inputs is stereotypical in each glomerulus (Hong and Wilson,
536 2015; Kazama and Wilson, 2008; Olsen et al., 2007; Yaksi and Wilson, 2010). PN plasticity could
537 theoretically arise from changes in any of these inputs, as well as changes in the intrinsic
538 biophysical properties of the PN that impact signal integration. The observation that chronic focal
539 activation of ORN input to a single glomerulus can elicit changes in PNs belonging to other
540 glomeruli suggests that olfactory plasticity is not glomerulus-autonomous and, at a minimum,
541 likely involves local lateral networks which mediate information flow across glomeruli. Prior

542 studies examining the mechanism of glomerulus-specific plasticity have suggested that some
543 genetically defined subsets of iLNs are important for mediating olfactory plasticity (Das et al.,
544 2011; Golovin and Broadie, 2016; Sachse et al., 2007). A significant unanswered question has
545 been how patterns of activity in the neurites of these iLNs, each of which ramify broadly in the
546 vast majority of antennal lobe glomeruli, are selectively modified to affect release sites present
547 in just one or a few glomeruli. Our observation that olfactory plasticity is not necessarily
548 glomerulus-specific is consistent with the broadly innervating anatomical characteristics of both
549 excitatory and inhibitory LNs.

550 Given the complexity of PN integration of direct and lateral inputs as well as prior reports
551 of glomerulus-specific plasticity in the antennal lobe, we considered the possibility that certain
552 elements in the circuit might be strongly affected by chronic odor exposure, but that these
553 changes might not be obvious due to compensatory modifications in other parts of the circuit.
554 For instance, prior work in fly found that chronic exposure to esters increased the sensitivity of
555 ORNs to these odors (Chakraborty et al., 2009; Iyengar et al., 2010), and multiple studies in
556 rodents have concluded that chronic odor exposure evokes plasticity in ORN responses (Cadiou
557 et al., 2014; Cavallin et al., 2010; Kass et al., 2013; Santoro and Dulac, 2012; Wang et al., 1993;
558 Watt et al., 2004). Note, however, that mammalian ORNs turn over constantly throughout the
559 lifetime of the animal, whereas insect ORNs do not. However, if, in addition to ORNs, another
560 circuit element such as lateral inhibition was concurrently affected by chronic odor exposure,
561 this scenario might obscure the ability to observe the impact of potential increases in
562 feedforward ORN excitation on PN responses. Thus, we directly measured how chronic odor
563 exposure impacts a number of key circuit mechanisms, including ORN odor responses, PN
564 intrinsic properties, ORN-PN synaptic strength, and lateral excitation. Overall, these circuit
565 features were remarkably stable to a major perturbation in the flies' olfactory environment. For
566 instance, the olfactory responses of ORNs in multiple glomeruli, as measured by single sensillum

567 extracellular recordings and by population calcium imaging, were unaffected by chronic
568 exposure to multiple odors and were stable across a wide range of odor concentrations.
569 Likewise, PN intrinsic properties and ORN-PN synaptic strength were similarly invariant to
570 chronic odor exposure. However, we did observe that the strength of lateral excitatory coupling
571 among glomeruli was increased in flies chronically exposed to the odor E2-hexenal. This finding
572 suggests a possible mechanism for the overall increased excitability of PNs in E2-hexenal
573 exposed flies, particularly in the weak stimulus regime in which lateral excitation has the most
574 impact (Yaksi and Wilson, 2010). Changes in the strength of lateral excitatory coupling between
575 eLNs and PNs have been previously implicated in the slow recovery of odor responses in PNs
576 that have chronically lost afferent ORN input due to injury (Kazama et al., 2011). Thus, the lateral
577 excitatory network might serve as a common substrate for olfactory plasticity in multiple
578 contexts.

579 The degree to which focal activation of a single ORN type (as occurs with low
580 concentrations of E2-hexenal or 2-butanone) recruits “intraglomerular” lateral excitation,
581 however, is unknown and requires further experimental validation. Additionally, not all odors
582 elicited enhanced lateral excitation in VA6 PNs after chronic odor exposure, suggesting that a
583 uniform global increase in the strength of eLN coupling to PNs cannot solely explain all of our
584 results. Indeed, although ORNs are probably the most important targets of GABAergic inhibition
585 in the antennal lobe, postsynaptic GABAergic inhibition onto PNs is also present (Horne et al.,
586 2018; Olsen and Wilson, 2008; Tobin et al., 2017) and may be variably recruited by different
587 odors and contribute to the lateral responses we measured. We propose that since feedforward
588 excitatory input is integrated with lateral excitatory and lateral inhibitory inputs in each
589 glomerulus in a complex and non-linear process, variation in the relative contributions of each of
590 these inputs may underlie some of the diversity in how chronic exposure to different odors
591 impacts odor coding in each glomerulus.

Implications for understanding experience-dependent changes in olfactory behavior

An important future direction is to determine how the specific odor exposure paradigm used in this study impacts olfactory preference and behavior towards the odor. A large number of studies in insect and in mammals have demonstrated that prior experience with an odor impacts how an animal subsequently responds to it. In flies, for instance, most studies have found that prior exposure to high concentrations of an odor (>~10^3 ppm in air) subsequently reduces the degree of behavioral aversion to high concentrations of that odor (Das et al., 2008; Devaud and Ferrus, 2003; Devaud et al., 2001; Sachse et al., 2007). In one study, however, where flies were chronically exposed to lower concentrations of odors (~1-10 ppm in air) that were demonstrated to be attractive to flies, experience with the odor further increased behavioral attraction towards it (Chakraborty et al., 2009). In preliminary experiments using strong attractive odor mixtures from natural fruit sources, our findings agree with this result (K.V.D. and E.J.H., personal communication). The divergent findings of these various studies may stem from exposure of flies to odors at different concentrations, to odors of different chemical identity, and/or to odors of differing behavioral meaning or valence. A still unanswered and important question is how olfactory plasticity depends on the properties of the odor environment, and, in particular, on whether the odor environment is pleasant or unpleasant for the animal. Since all odors, both attractive and aversive, are effectively aversive at very high concentrations, many past studies do not explicitly address this question.

Prior studies have suggested that experience-dependent modification of olfactory behavior in fly stems from odor-specific changes in the structure and function of the antennal lobe, which act to adapt early olfactory codes to more efficiently encode the frequency with which odors are present in the local environment (Chakraborty et al., 2009; Das et al., 2011; Devaud et al., 2001; Kidd et al., 2015; Sachse et al., 2007). The results of this study, taken

617 together with the inability to establish a consistent set of rules for predicting how olfactory
618 plasticity will impact antennal lobe coding, argue against this hypothesis. Indeed, given that most
619 typical odors are broadly encoded across many glomeruli, glomerulus-selective plasticity in the
620 antennal lobe would seem to be an inefficient substrate for odor-specific plasticity since most
621 individual glomeruli participate in the representation of many different odors. Rather than
622 representing a design feature of the circuit, modest shifts in PN responses driven by chronic
623 odor exposure may rather reflect imperfections in a system that is principally designed to
624 maintain stable stimulus representations at the earliest stages of odor processing. If this is the
625 case, odor experience-dependent changes in olfactory behavior in flies are likely to rather arise
626 from plasticity downstream of the antennal lobe. One higher order olfactory area which receives
627 antennal lobe output, the mushroom body, has been extensively studied for its role in associative
628 learning (Heisenberg, 2003). Indeed, chronic odor exposure experiments are nearly always, by
629 necessity, carried out in the presence of food, which may signal to flies a positive value of the
630 environment and become associated with the odor. More work is needed to evaluate how
631 behavioral plasticity elicited by chronic odor exposure may depend on additional features of the
632 environment, for instance, if exposure occurs in a passive versus rewarding (or aversive) context.
633
634 **Implications for general principles of sensory plasticity**
635 The stability of odor responses in early olfactory processing areas, even when challenged
636 with persistent perturbations in the sensory environment, may reflect a more general design
637 principle of sensory circuits. Even in mammalian nervous systems, which exhibit an overall higher
638 degree of neural plasticity than insect systems, the function of early stages of sensory processing
639 closer to the periphery is less dependent on normal sensory experience than later stages of
640 cortical processing. For example, although normal visual experience is a well-established
641 requirement for normal topographic maps, orientation selectivity, and direction selectivity in

642 higher visual areas (Cang and Feldheim, 2013; Espinosa and Stryker, 2012; Huberman et al.,
643 2008), the structure and function of retinal circuitry is much less impacted by abnormal visual
644 experience (D'Orazi et al., 2014; Elstrott and Feller, 2009). To take the case of direction
645 selectivity as an example, whereas raising animals in the dark prevents the emergence of
646 direction-selective responses in primary visual cortex (Li et al., 2006, 2008), direction-selective
647 ganglion cells in the retina have mature responses at birth, and have normal directional tuning,
648 speed tuning, and anatomy in dark-reared animals (Chan and Chiao, 2008; Elstrott and Feller,
649 2009; Elstrott et al., 2008). Similarly, in the human auditory system, cochlear tuning is essentially
650 mature at birth, but brainstem and cortical auditory responses exhibit significant plasticity in
651 postnatal life, consistent with auditory experience having a bigger impact on the function of
652 higher order auditory circuits (Moore and Linthicum, 2007; Sanes and Bao, 2009). Thus, in both
653 insects and vertebrates, experience-independent processes, specified by developmental
654 genetic programs, appear to dominate in determining the structure and function of early stages
655 of sensory processing, with the role of sensory experience becoming more prominent in higher-
656 order stages of processing.

657 Why might plasticity be limited in early stages of sensory processing? Neural plasticity,
658 like any form of phenotypic plasticity, comes at a cost. For instance, plasticity at the sensory
659 periphery could be subject to an information acquisition cost, stemming from poor reliability or
660 undersampling of the stimuli being used to evaluate the statistical structure of the environment.
661 Unreliable information about the environment could result in potentially even more inefficient
662 sensory coding. Another potential cost of plasticity could arise from temporal mismatching, for
663 instance, if the stimulus structure of the environment were to shift more rapidly than the time
664 scale over which neural plasticity could be implemented. Generating a stable representation of
665 the world at early stages of processing, which is invariant to local shifts in the stimulus
666 environment, may be the best strategy. The initial sensory representation is usually relayed to

667 multiple higher order processing areas, each of which may use the sensory information for
668 different behavioral tasks. Allowing neural plasticity to rather impinge on later stages of
669 processing may allow each different downstream circuit to independently reformat the sensory
670 representation in way that best subserves its specialized function.

671

672 # SUPPLEMENTARY MATERIALS

673 **Supplemental Table 1: Complete genotypes and *n* for all experiments.**
674 Solvent is paraffin oil.

FIGURE	GENOTYPE	EXPERIMENTAL GROUP	STIMULUS	NO. FLIES (*N*)
1C-D	*np3481-gal4, UAS-cd8:gfp* (X)	E2-hexenal	solvent	1
			E2-hexenal, 10^{-7}	1
2**B-F**	*np3481-gal4, UAS-cd8:gfp* (X)	E2-hexenal	solvent	3
2Q		exposed	E2-hexenal, 10^{-12}	3
			E2-hexenal, 10^{-11}	5
			E2-hexenal, 10^{-10}	**9**
			E2-hexenal, 10^{-9}	**10**
			E2-hexenal, 10^{-8}	**11**
			E2-hexenal, 10^{-7}	**12**
			E2-hexenal, 10^{-6}	10
			E2-hexenal, 10^{-5}	6
		solvent exposed	solvent	3
			E2-hexenal, 10^{-12}	3
			E2-hexenal, 10^{-11}	3
			E2-hexenal, 10^{-10}	**8**
			E2-hexenal, 10^{-9}	**7**
			E2-hexenal, 10^{-8}	**19**
			E2-hexenal, 10^{-7}	**19**
			E2-hexenal, 10^{-6}	14
			E2-hexenal, 10^{-5}	9
2**H-J**	*np3481-gal4, UAS-cd8:gfp* (X)	2-butanone	2-butanone, 10^{-8}	4
2R		exposed	**2-butanone, 10^{-7}**	**11**
3F			**2-butanone, 10^{-6}**	**12**
			2-butanone, 10^{-5}	**13**
			2-butanone, 10^{-4}	**12**
		solvent exposed	2-butanone, 10^{-8}	6
			2-butanone, 10^{-7}	**16**
			2-butanone, 10^{-6}	**13**
			2-butanone, 10^{-5}	**14**

			2-butanone, 10^{-4}	**11**
2L-P 2S	*UAS-cd8:gfp* (X)*; mz612-gal4, UAS-cd8:gfp* (II)	geranyl acetate exposed	geranyl acetate, 10^{-7}	7
			geranyl acetate, 10^{-6}	9
			geranyl acetate, 10^{-5}	9
			geranyl acetate, 10^{-4}	8
		solvent exposed	geranyl acetate, 10^{-7}	10
			geranyl acetate, 10^{-6}	11
			geranyl acetate, 10^{-5}	11
			geranyl acetate, 10^{-4}	8
3B-E 3G-H	*np3481-gal4, UAS-cd8:gfp* (X)	E2-hexenal exposed	2-butanone, 10^{-7}	6
			2-butanone, 10^{-6}	8
			2-butanone, 10^{-5}	7
			2-butanone, 10^{-4}	5
		solvent exposed	2-butanone, 10^{-7}	16
			2-butanone, 10^{-6}	13
			2-butanone, 10^{-5}	14
			2-butanone, 10^{-4}	11
3J-N	*UAS-cd8:gfp* (X)*; mz612-gal4, UAS-cd8:gfp* (II)	E2-hexenal exposed	geranyl acetate, 10^{-7}	5
			geranyl acetate, 10^{-6}	5
			geranyl acetate, 10^{-5}	5
			geranyl acetate, 10^{-4}	5
		solvent exposed	geranyl acetate, 10^{-7}	10
			geranyl acetate, 10^{-6}	11
			geranyl acetate, 10^{-5}	11
			geranyl acetate, 10^{-4}	8
4B-C	*np3481-gal4, UAS-cd8:gfp* (X)	2-butanone exposed	*pentyl acetate, 10^{-3}*	
			+2-butanone, 10^{-8}	3
			+2-butanone, 10^{-7}	7
			+2-butanone, 10^{-6}	6
			+2-butanone, 10^{-5}	7
			+2-butanone, 10^{-4}	6
		solvent exposed	*pentyl acetate, 10^{-3}*	
			+2-butanone, 10^{-8}	6
			+2-butanone, 10^{-7}	6
			+2-butanone, 10^{-6}	6
			+2-butanone, 10^{-5}	7
			+2-butanone, 10^{-4}	5
4E-F	*np3481-gal4, UAS-cd8:gfp* (X)	E2-hexenal exposed	*pentyl acetate, 10^{-3}*	
			+2-butanone, 10^{-8}	3
			+2-butanone, 10^{-7}	3
			+2-butanone, 10^{-6}	4
			+2-butanone, 10^{-5}	3
			+2-butanone, 10^{-4}	3

		solvent exposed	*pentyl acetate, 10^{-3}*	
			+2-butanone, 10^{-8}	6
			+2-butanone, 10^{-7}	6
			+2-butanone, 10^{-6}	6
			+2-butanone, 10^{-5}	7
			+2-butanone, 10^{-4}	5
5A	*+/UAS-brp.S-mStraw* (II)*; 20XUAS-cd8:gfp/np3056-gal4* (III)	solvent exposed	NA	1
5B 5D 5F 5H	*+/UAS-brp.S-mStraw* (II)*; 20XUAS-cd8:gfp/np3056-gal4* (III)	2-butanone exposed	NA	13
		solvent exposed	NA	10
5C 5E 5G 5I	*+/UAS-brp.S-mStraw* (II)*; 20XUAS-cd8:gfp/np3056-gal4* (III)	E2-hexenal exposed	NA	11
		solvent exposed	NA	8
6B 6C	*np3481-gal4, UAS-cd8:gfp* (X)	E2-hexenal exposed	solvent	12
			E2-hexenal, 10^{-12}	11
			E2-hexenal, 10^{-11}	11
			E2-hexenal, 10^{-10}	10
			E2-hexenal, 10^{-9}	10
			E2-hexenal, 10^{-8}	8
			E2-hexenal, 10^{-7}	9
			E2-hexenal, 10^{-6}	9
			E2-hexenal, 10^{-5}	9
			E2-hexenal, 10^{-4}	10
		solvent exposed	solvent	9
			E2-hexenal, 10^{-12}	9
			E2-hexenal, 10^{-11}	9
			E2-hexenal, 10^{-10}	8
			E2-hexenal, 10^{-9}	8
			E2-hexenal, 10^{-8}	9
			E2-hexenal, 10^{-7}	9
			E2-hexenal, 10^{-6}	7
			E2-hexenal, 10^{-5}	6
			E2-hexenal, 10^{-4}	6
6E 6F	*np3481-gal4, UAS-cd8:gfp* (X)	2-butanone exposed	solvent	6
			2-butanone, 10^{-10}	9
			2-butanone, 10^{-9}	9
			2-butanone, 10^{-8}	9
			2-butanone, 10^{-7}	10
			2-butanone, 10^{-6}	10

			2-butanone, 10^{-5}	9
			2-butanone, 10^{-4}	10
			2-butanone, 10^{-3}	9
		solvent exposed	solvent	9
			2-butanone, 10^{-10}	11
			2-butanone, 10^{-9}	10
			2-butanone, 10^{-8}	10
			2-butanone, 10^{-7}	10
			2-butanone, 10^{-6}	9
			2-butanone, 10^{-5}	9
			2-butanone, 10^{-4}	9
			2-butanone, 10^{-3}	9
6H 6I	*np3481-gal4, UAS-cd8:gfp* (X)	E2-hexenal exposed	solvent	5
			2-butanone, 10^{-10}	9
			2-butanone, 10^{-9}	9
			2-butanone, 10^{-8}	9
			2-butanone, 10^{-7}	9
			2-butanone, 10^{-6}	9
			2-butanone, 10^{-5}	8
			2-butanone, 10^{-4}	8
			2-butanone, 10^{-3}	9
		solvent exposed	solvent	9
			2-butanone, 10^{-10}	11
			2-butanone, 10^{-9}	10
			2-butanone, 10^{-8}	10
			2-butanone, 10^{-7}	10
			2-butanone, 10^{-6}	9
			2-butanone, 10^{-5}	9
			2-butanone, 10^{-4}	9
			2-butanone, 10^{-3}	9
6K	*+/or7a-gal4*(KI) (X)*; +/20XUAS-IVS-syn21-opGCaMP6f-p10* (II)	solvent exposed	E2-hexenal, 10^{-7}	1
6L 6M	*+/or7a-gal4*(KI) (X)*; +/20XUAS-IVS-syn21-opGCaMP6f-p10* (II)	E2-hexenal exposed	solvent	8
			E2-hexenal, 10^{-12}	6
			E2-hexenal, 10^{-11}	8
			E2-hexenal, 10^{-10}	8
			E2-hexenal, 10^{-9}	8
			E2-hexenal, 10^{-8}	8
			E2-hexenal, 10^{-7}	7
			E2-hexenal, 10^{-6}	8
		solvent exposed	solvent	8
			E2-hexenal, 10^{-12}	6
			E2-hexenal, 10^{-11}	8
			E2-hexenal, 10^{-10}	8

			E2-hexenal, 10^{-9}	8
			E2-hexenal, 10^{-8}	8
			E2-hexenal, 10^{-7}	7
			E2-hexenal, 10^{-6}	8
7B-C	*np3481-gal4, UAS-cd8:gfp* (X)	E2-hexenal exposed	NA	4
		solvent exposed	NA	4
7E	*np3481-gal4, UAS-cd8:gfp* (X)*; +/13xlexAop2-IVS-CsChrimson.mVenus* (II); *+/or7a-lexA* (III)	solvent exposed	NA	1
7F-G	*np3481-gal4, UAS-cd8:gfp* (X)*; +/13xlexAop2-IVS-CsChrimson.mVenus* (II); *+/or7a-lexA* (III)	E2-hexenal exposed	NA	5
		solvent exposed	NA	7
7I-J	*UAS-cd8:gfp* (X)*; mz612-gal4, UAS-cd8:gfp* (II)	E2-hexenal exposed	solvent	3
			pentyl acetate	3
			2-heptanone	3
			E2-hexenal	3
			isobutyl acetate	3
			p-cresol	3
			2-butanone	3
		solvent exposed	solvent	3
			pentyl acetate	5
			2-heptanone	4
			E2-hexenal	4
			isobutyl acetate	4
			p-cresol	4
			2-butanone	3

675

676

677

678

679

680

681

Figure 2 – figure supplement 1: Examples of resampling analysis for determination of p-values in Figure 2.
A) Histograms of the difference between group means in the 10,000 permuted datasets of odor-evoked depolarization in DL5 PNs from E2-hexenal- or solvent-exposed flies (from **Figure 2C**). For each stimulus, the labels that assign each data point (from a single PN) to the odor- or solvent-exposed group were randomly shuffled 10,000 times without replacement, reassigning each data point to either the odor- or solvent-exposed group but retaining the number of resampled observations in each group. The distribution of the difference between the means of the groups in the 10,000 permutations is plotted. The red dotted line marks the position of the observed difference between odor- and solvent-exposed groups ($\mu_{odor\ exposed} - \mu_{solv\ exposed}$); the black dotted line marks the position of ($\mu_{solv\ exposed} - \mu_{odor\ exposed}$). The p-value for each comparison is computed as the fraction of absolute resampled differences larger than the absolute observed difference (e.g., the fraction of the distribution lying outside the dotted bounds).
B-E) Same as **A)**, but for odor-evoked firing rate in DL5 PNs from E2-hexenal- or solvent-exposed flies (from **Figure 2E**) **(B)**; odor-evoked depolarization in VM7 PNs from 2-butanone- or solvent-exposed flies (from **Figure 2I**) **(C)**; odor-evoked depolarization in VA6 PNs from geranyl acetate- or solvent-exposed flies (from Figure **2M**) **(D)**; and odor-evoked firing rate in VA6 PNs from geranyl acetate- or solvent-exposed flies (from **Figure 2O**) **(E)**.

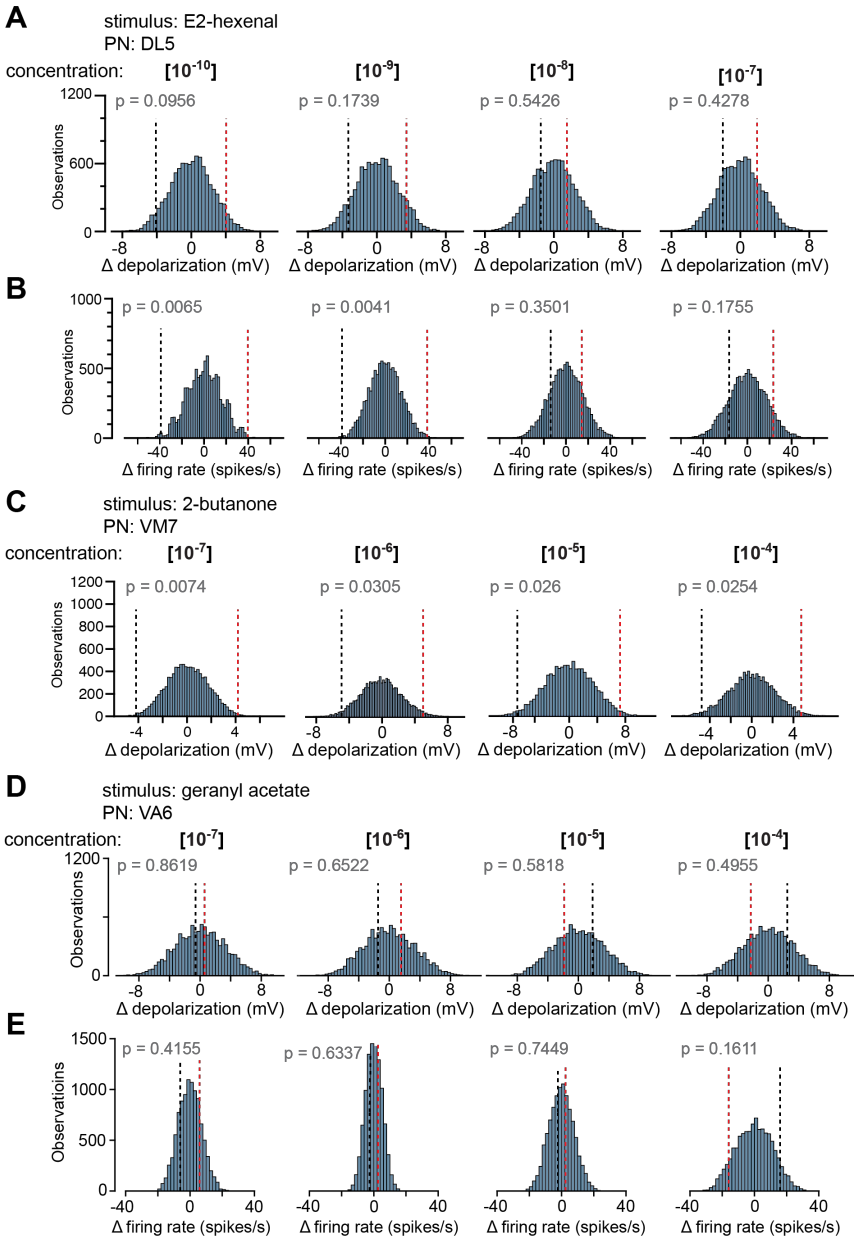

Figure 6 – figure supplement 1: Statistical analysis of spontaneous and odor-evoked ORN firing rates in odor- and solvent-exposed flies.

Statistical analysis is the same as in **Figure 2 – figure supplement 1**.

A-D) Histograms of the difference between group means in 10,000 permutations of the datasets for each indicated comparison of odor-evoked firing rates in **A)** ab4a ORNs from E2-hexenal- or solvent-exposed flies (from **Figure 6B**); **B)** pb1a ORNs from 2-butanone- or solvent-exposed flies (from **Figure 6E**); **C)** pb1a ORNs from E2-hexenal- or solvent-exposed flies (from **Figure 6H**); and **D)** odor-evoked calcium signals from ab4a ORN axon terminals in E2-hexenal- or solvent-exposed flies (from **Figure 6L**). The p-value for each comparison is computed as the fraction of absolute resampled differences larger than the absolute observed difference (e.g., the fraction of the distribution lying outside the dotted bounds).

E-G) Mean spontaneous firing rate, and statistical comparison of means, computed over a 5 s window prior to stimulus onset in ORNs corresponding to each condition in **A-C)**.

H) Mean resting fluorescence computed over a 5 s window prior to stimulus onset in ab4a ORN terminals in the DL5 glomerulus in E2-hexenal- and solvent-exposed flies. None of the comparisons in **Figure 6** between odor- and solvent-exposed groups are statistically significant at the α=0.05 level (with Bonferroni adjustment for multiple comparisons).

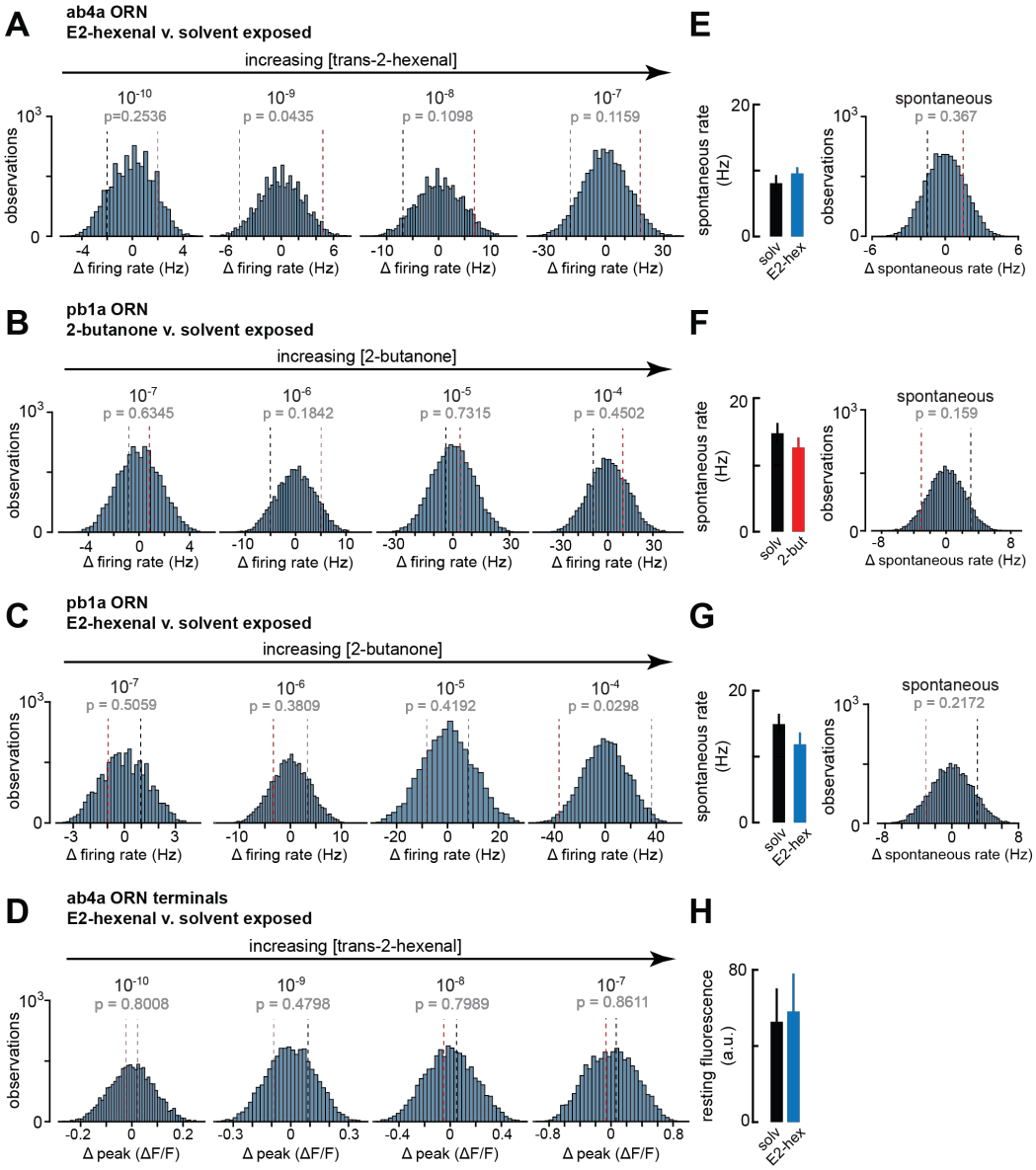

Figure 7- figure supplement 1: PN intrinsic properties and latency of light-evoked EPSCs.
A) Membrane potential versus current for increasing steps of current injection (from **Figure 7B**) in deafferented DL5 PNs from E2-hexenal- and solvent-exposed flies.
B) Same as **A)** but plotting firing rate versus membrane potential at each current step.
C) EPSCs evoked by a 100 µs pulse of light (488 nm, ~0.175 mW/mm^2) in a deafferented DL5 PN from a solvent-reared fly expressing CsChrimson in presynaptic ab4a ORNs. Note the variable latency to the peak of the evoked EPSC, which is consistent with the approximate latency of the first light-evoked spike in ORN recordings from in the antenna. EPSCs are aligned by their peaks for averaging across trials in **Figure 7E-G**.

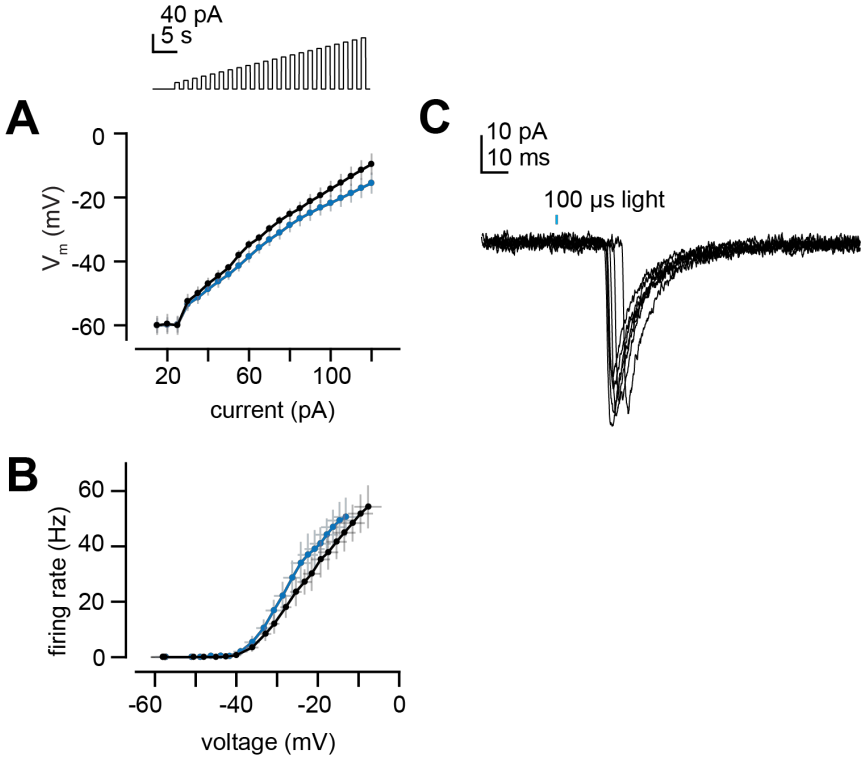

682

683 # METHODS

684 ## Flies

685 *Drosophila melanogaster* were raised on a 12:12 light:dark cycle at 25°C and 70% relative
686 humidity on cornmeal/molasses food containing: water (17.8 l), agar (136 g), cornmeal (1335.4
687 g), yeast (540 g), sucrose (320 g), molasses (1.64 l), $CaCl_2$ (12.5 g), sodium tartrate (150 g),
688 tegosept (18.45 g), 95% ethanol (153.3 ml) and propionic acid (91.5 ml). All experiments were
689 performed in 2-day old female flies. The specific genotype of the flies used in each experiment
690 are given in Supplemental Table 1. The transgenes used in this study were acquired from the

691 Bloomington Drosophila Stock Center (BDSC) or the Kyoto Drosophila Stock Center (DGGR),
692 unless otherwise indicated. They have been previously characterized as follows: *np3481-gal4*
693 (Kyoto:113297) labels DL5 and VM7 PNs (Hayashi et al., 2002; Olsen et al., 2007); *mz612-gal4*
694 (II) (gift of L. Luo) labels VA6 PNs (Marin et al., 2005); *or7a-gal4*(KI) (gift of C. Potter) expresses
695 Gal4 from the *or7a* locus under the control of its endogenous regulatory elements (Lin et al.,
696 2015); *UAS-cd8:gfp* (X) (RRID:BDSC_5136) and *UAS-cd8:gfp* (II) (RRID:BDSC_5137) express
697 CD8-tagged GFP, which is targeted to the membrane, under Gal4 control (Lee and Luo, 1999);
698 *20xUAS-IVS-cd8:gfp* (attP2) (RRID:BDSC_32194) expressed CD8-tagged GFP under Gal4
699 control (Pfeiffer et al., 2010)*; UAS-brp.S-mStrawberry* (II) (gift of S. Sigrist) expresses a red
700 fluorescent protein-tagged short-form of bruchpilot (Fouquet et al., 2009); *20xUAS-IVS-syn21-*
701 *opGCaMP6f-p10* (su(Hw)attP5) (gift of B. Pfeiffer and D. Anderson) expresses codon-optimized
702 GCaMP6f under Gal4 control (Chen et al., 2013); and *13xlexAop2-IVS-CsChrimson.mVenus*
703 (attP40) (RRID:BDSC_55138) expresses a Venus-tagged red-shifted channelrhodopsin
704 CsChrimson under lexA control (Klapoetke et al., 2014).
705
706 *or7a-lexA* (III) flies were generated as follows. The *or7a* promoter was PCR amplified from a
707 bacterial artificial chromosome (RPCI-98 library, clone 39F18, BACPAC Resources) containing
708 the *or7a* locus of *D. melanogaster* using primers 5'-ACCGCATCCCGATCAAGACACAC-3' and
709 5'-TGATGGACTTTTGACGCCTGGGAATA-3'. The *or7a* promoter was inserted 5' to *nlslexA::p65*
710 using isothermal assembly in vector *pBPnlslexA::p65Uw*, replacing the ccdB cassette. The
711 plasmid *pBPnlslexA::p65Uw* was a gift from G. Rubin (Addgene plasmid #26230,
712 RRID:Addgene_26230). The final sequence of the construct was confirmed by Sanger
713 sequencing, and transgenic flies were generated by site-specific integration into the VK00027
714 landing site (BestGene, Inc., Chino Hills, CA). To verify the selectivity of the driver, *or7a-lexA* was
715 crossed to *13xlexAop2-mCD8:gfp* (RRID:BDSC_32205), and brains of the resulting progeny flies

716 (2 days old) were dissected and immunostained with antibodies against GFP and nc82. GFP
717 expression was observed selectively in ab4a ORN axons projecting to the DL5 glomerulus; no
718 other signal was observed in the central brain.
719
720 **Chronic odor exposure**
721 Flies were chronically exposed to specific monomolecular odors while reared in standard fly
722 bottles containing cornmeal/molasses food and sealed with modified cotton plugs through which
723 two thin-walled stainless-steel hollow rods (~5 cm length, ~3.2 mm inner diameter) were tightly
724 inserted, serving as an inlet and an outlet for air flow. The bottom of the cotton plug was lined
725 with mesh (McMaster-Carr #9318T45) to prevent flies from entering the rods. The inlet port was
726 fit with a luer connector for easy connection to the carrier stream; the outlet port was vented with
727 loose vacuum suction.
728 The odor environment inside the bottle was controlled by delivering to the inlet of the
729 bottle a stream of charcoal-filtered, humidified air (275 ml/min), with a small fraction of the air
730 stream (odor stream, 25 ml/min) diverted into the headspace of a control vial filled with solvent
731 (paraffin oil, J.T. Baker, VWR #JTS894-7) before it was reunited with the carrier stream (250
732 ml/min). Air flow rates were controlled using variable area valved flow meters (Cole-Parmer). In
733 response to an external 5V command, a three-way solenoid valve redirected the 25 ml/min odor
734 stream from the headspace of the control solvent vial through the headspace of the vial
735 containing diluted odor for 1 second. The diluted odor was continuously stirred using a miniature
736 magnetic stir bar and sir plate (homebrewing.org). Delivery of the 1-second pulse of odor into
737 the carrier stream was repeated every 21 seconds. Tygon tubing (E-3603) was used throughout
738 the odor delivery system, with the exception of a portion of the carrier stream where odor entered
739 and the path from the odor vial to the input to the carrier stream, where PTFE tubing was used.

740 The stability of the amplitude of the odor pulse over the course of 24 hours was measured
741 using a photoionization detector (200B miniPID, Aurora Instruments), with the sensor probe
742 mounted at the center of a fresh fly bottle. Based on the observed rundown in the amplitude of
743 the odor pulse (Figure 1B), the odor vial in the odor delivery system was swapped out every 12
744 hours for a fresh dilution of odor during chronic exposure experiment with flies. Under these
745 conditions, the amplitude of the odor pulse was not expected to decrease more than ~10% at
746 any point during the exposure period.

747 Flies were seeded in a fresh fly bottle at low density (~7-8 females). The evening prior to
748 expected eclosion, any adult flies were removed from the bottle, and controlled odor delivery
749 was initiated into the bottle. The next morning (day 0), newly eclosed flies were transferred into
750 a fresh bottle and controlled odor delivery was continued for another ~48 hours. Experiments
751 were typically conducted on day 2.

752 Odor concentrations in this study are referred to by the v/v dilution factor of the odor in
753 paraffin oil in the odor vial. For chronic odor exposure, flies were exposed to odors at dilution
754 factors of 10^{-7} for E2-hexenal, 10^{-4} for 2-butanone, and 10^{-4} for geranyl acetate. Headspace
755 concentrations were further diluted 1:11 in air prior to delivery to the fly bottle. Flies were
756 chronically exposed to pulses of odor (in gas phase) that are estimated from published vapor
757 pressure data at 25ºC (Kim et al., 2021) to be ~1 ppb for E2-hexenal (10^{-7}), ~13 ppm for 2-
758 butanone (10^{-4}), and ~4 ppb for geranyl acetate (10^{-4}).

759 The mean spontaneous firing rates of the PNs (DL5, VM7, VA6) investigated in this study
760 range from ~3-7 Hz, and each 1-sec odor pulse delivered during chronic odor exposure elicits
761 ~150 spikes in PNs (Figure 1). Thus, chronic odor exposure approximately doubles overall PN
762 firing rates (from ~180-420 spikes/min to 690-930 spikes/min) and elicits ~1.3 million extra spikes
763 in a specific PN type over the course of two days.

764

765 **Electrophysiological recordings**

766 *PN recordings*

767 Electrophysiological measurements were performed on 2 day-old female flies essentially as
768 previously described (Wilson et al., 2004). Flies were briefly cold-anesthetized and immobilized
769 using wax. The composition of the internal pipette solution for current clamp recordings in PNs
770 was (in mM): potassium aspartate 140, HEPES 10, MgATP 4, Na_3GFP 0.5, EGTA 1, KCl 1,
771 biocytin hydrazide 13. The internal solution was adjusted to a pH of 7.3 with KOH or aspartic
772 acid and an osmolarity between 262-268 mOsm. For voltage-clamp recordings, an equal
773 concentration of cesium was substituted for potassium. The external solution was Drosophila
774 saline containing (in mM): NaCl 103, KCl 3, N-tris(hydroxymethyl) methyl-2-aminoethane-sulfonic
775 acid 5, trehalose 8, glucose 10, $NaHCO_3$ 26, NaH_2PO_4 1, $CaCl_2$ 1.5, $MgCl_2$ 4. The pH of the
776 external solution was adjusted to 7.2 with HCl or NaOH (when bubbled with 95% O_2/5% CO_2),
777 and the osmolarity was adjusted to ~270-275 mOsm. Recording pipettes were fabricated from
778 borosilicate glass and had a resistance of ~6-8 MΩ. Recordings were acquired with a MultiClamp
779 700B (Axon Instruments) using a CV-7B headstage (500 MΩ). Data were low-pass filtered at 5
780 kHz, digitized at 10 kHz, and acquired in MATLAB (Mathworks, Natick, MA). Voltages are
781 uncorrected for liquid junction potential.

782 Flies were removed from the odor exposure environment at least one hour prior to
783 recordings, briefly cold-anesthetized anesthetized, and recordings were performed at room
784 temperature. Recordings with respect to experimental groups (odor-exposed versus solvent-
785 exposed) were conducted in a quasi-randomized order; the experimenter was not masked to
786 experimental condition. For experiments in Figure 7, the antennal nerves were bilaterally severed
787 immediately prior to recordings using fine forceps. PN somata were visualized with side
788 illumination form an infrared LED (Smartvision) under a 40x water immersion objective on an
789 upright compound microscope equipped with an epifluorescence module and 488 nm blue light

source (Sutter Lambda TLED+). Whole-cell patch-clamp recordings were targeted to specific PNs types based on GFP fluorescence directed by genetic drivers. Three PN types were targeted in this study: DL5 and VM7 using *np3481-gal4* and VA6 using *mz612-gal4*. One neuron was recorded per brain. PN identity was confirmed using diagnostic odors, and the morphology (and thus identity) of all PNs was further verified posthoc by streptavidin staining in fixed brains. Cells with little or no spontaneous activity upon break-in, suggesting antennal nerve damage, were discarded. Input resistance was monitored on every trial in real-time, and recordings were terminated if the input resistance of the cell drifted by more than 20%.

ORN recordings

Single-sensillum recordings were performed essentially as previously described (Bhandawat et al., 2007). Flies were removed from the odor exposure environment at least one hour prior to recordings, briefly cold-anesthetized, and recordings were performed at room temperature. Briefly, flies were immobilized in the end of a trimmed pipette tip using wax, and one antenna or one palp was visualized under a 50x air objective. The antenna was stabilized by tightly sandwiching it between a set of two fine glass hooks, fashioned by gently heating pipettes pulled from glass capillaries (World Precision Instruments, TW150F-3). The palp was stabilized from above with a fine glass pipette pressing it firmly against a glass coverslip provided from below. A reference electrode filled with external saline (see above) was inserted into the eye, and a sharp saline-filled glass recording microelectrode was inserted into the base of the selected sensillum under visual control. Recordings from ab4 and pb1 sensilla were established in the antenna and palp, respectively, based on the characteristic size and morphology of the sensillum, its position on the antenna, and the presence of two distinct spike waveforms, each having a characteristic odor sensitivity and spontaneous firing frequency (de Bruyne et al., 2001). Signals were acquired with a MultiClamp 700B amplifier, low-pass filtered at 2 kHz, digitized at 10 kHz, and acquired in

MATLAB. Single-sensillum recordings were performed in 2-day old *np3481-gal4, UAS-cd8:gfp* females to allow direct comparisons to PN data.

Odor stimuli

Odors used in this study were benzaldehyde, 2-butanone, *p*-cresol, geosmin, geranyl acetate, 2-heptanone, E2-hexenal, isobutyl acetate, and pentyl acetate. All odors were obtained from MilliporeSigma or Fisher Scientific at the highest purity available (typically >99%). Odor stimuli are referred to by their v/v dilution factor in paraffin oil. Each 20-ml odor vial contained 2 ml of diluted odor in paraffin oil. Diagnostic stimuli that distinguished targeted PN types from other labeled PN types in the driver line used were as follows: for DL5 PNs, E2-hexenal (10^{-8}) and benzaldehyde (10^{-4}); for VM7 PNs, 2-butanone (10^{-7}) and isobutyl acetate (10^{-4}); and for VA6 PNs, geranyl acetate (10^{-6}). Diagnostic stimuli for ORN classes were as follows: for the ab4 sensillum on the antenna, E2-hexenal (10^{-7}) for the ab4a "A" spike and geosmin (10^{-2}) for the ab4b "B" spike; and for the pb1 sensillum on the palp, 2-butanone (10^{-5}) for the pb1a "A" spike and *p*-cresol (10^{-3}) for the pb1b "B" spike.

Fresh odor dilutions were made every 5 days. Each measurement in a fly represents the mean of 5 trials for ORN responses or 6 trials for PN responses, spaced 40 seconds apart. Solvent (paraffin oil) trials were routinely interleaved to assess for contamination. Stimuli were presented in pseudo-randomized order, except for measurements of concentration-response curves where odors were presented from low to high concentrations.

Odors were presented during recordings from olfactory neurons essentially as previously described (Bhandawat et al., 2007). In brief, a constant stream of charcoal-filtered air (2.22 L/min) was directed at the fly, with a small portion of the stream (220 mL/min) passing through the headspace of a control vial filled with paraffin oil (solvent) prior to joining the carrier stream (2.0 L/min). Air flow was controlled using mass flow controllers (Alicat Scientific). When triggered by

an external voltage command, a three-way solenoid valve redirected the small portion of the stream (220 mL/min) from the solvent vial through the headspace of a vial containing odor for 500 ms; thus, the concentration of the odor in gas phase was further diluted ~10-fold prior to final delivery to the animal. The solvent vial and the odor vial entered the carrier stream at the same point, ~10 cm from the end of the tube. The tube opening measured ~4 mm in diameter and was positioned ~1 cm away from the fly. We presented 500-ms pulses of odor unless otherwise indicated.

Odor mixtures (Figure 4) were generated by mixing in air. In these experiments, a second solenoid valve was added that diverted another small fraction of the carrier stream (220 ml/min) through either a second solvent vial or a second odor vial before rejoining the carrier stream. When the two solenoids were both triggered, they drew from the carrier stream at the same point, and the two odorized streams also both rejoined the carrier stream at about the same point, ~10 cm from the end of the delivery tube.

Immunohistochemistry

Intracellular biocytin fills were processed as previously described (Wilson et al., 2004). In brief, brains were fixed for 14 min at room temperature in freshly prepared 4% paraformaldehyde, incubated overnight in mouse nc82 primary antibody (1:40, Developmental Studies Hybridoma Bank #AB_2314866), then subsequently incubated overnight in Alexa Fluor 568 streptavidin conjugate (1:1000, Molecular Probes) and Alexa Fluor 633 goat anti-mouse (1:500, Molecular Probes). PN morphologies were reconstructed from serial confocal images through the brain at 40X magnification and 1-µm step size.

LN innervation was quantified in flies of genotype *+/UAS-brp.S-mStraw; 20XUAS-IVS-cd8:gfp/np3056-gal4*; the *brp.S-mStraw* signal was not measured. Immediately after dissection, brains were fixed for 14 min in freshly prepared 4% paraformaldehyde and

incubated overnight in rat anti-CD8 (1:50, Thermo Fisher #MA5-17594) and mouse nc82 (1:40) primary antibodies, then subsequently incubated overnight in Alexa Fluor 488 goat anti-rat (1:500, Abcam #ab150157) and Alexa Fluor 633 goat anti-mouse (1:500, Thermo Fisher #A21050) secondary antibodies. All steps were performed at room temperature, and brains were mounted and imaged in Vectashield mounting medium (Vector labs). In pilot experiments, we compared direct GFP fluorescence in lightly fixed brain with amplified GFP signal using the standard protocol and observed weaker, but qualitatively similar signals. Confocal z-stacks at 1024x1024 resolution spanning the entire volume of the antennal lobe were collected on a Leica SP8 confocal microscope at 1 μm slice intervals using a 63× oil-immersion lens. Identical laser power and imaging settings were used for all experiments.

Calcium imaging

Calcium imaging of ab4a ORN terminals in the DL5 glomerulus was performed on 2-day old female flies essentially as previously described (Hong and Wilson, 2015). In brief, flies were cold-anesthetized and immobilized with wax. The antennal lobes were exposed by removal of the dorsal flap of head cuticle, and the brain was perfused with Drosophila saline (see above) that was cooled to 21ºC (TC-324C, Warner Instruments) and circulated at a rate of 2-3 ml/min. GCaMP6f signals were measured on a two-photon microscope (Thorlabs, Sterling, VA) using a Ti-Sapphire femtosecond laser (MaiTai eHP DS, Spectra-Physics) at an excitation wavelength of 925 nm, steered by a galvo-galvo scanner. Images were acquired with a 20x water-immersion objective (XLUMPLFLN, Olympus) at 256x96 pixels, a frame rate of 11 Hz, and a dwell time of 2μs/pixel. The same laser power and imaging settings were maintained for all experiments. The microscope and data acquisition were controlled using ThorImage 3.0. The DL5 glomeruli were clearly labeled as bilateral spherical structures ~10 μm from the dorsal surface of the antennal lobes. In each trial, an 8 s period of baseline activity was collected immediately prior to stimulus

890 presentation which was used to establish the level of baseline fluorescence of each pixel. Each
891 odor stimulus was presented for 500 ms, for three trials, with a 45-s interstimulus interval.
892
893 **Optogenetic stimulation of ORN axons**
894 A stock solution of all-trans-retinal (Sigma-Aldrich, R2500) was prepared at 35 mM in
895 95% ethanol and stored at -20° C in the dark. The cross that generated the experimental flies
896 was maintained in the dark. Newly eclosed experimental flies for optogenetic experiments were
897 transferred to standard cornmeal/molasses food supplemented with 350 μM all-trans-retinal
898 mixed into the food and exposed to odor (or solvent) for two days in the dark.
899 After exposing the antennal lobes, the antennal nerves were acutely and bilaterally
900 severed at their distal entry point into the first segment of the antennal, eliminating EPSCs
901 derived from spontaneous ORN spiking. Electrophysiology rigs were light-proofed. Whole-cell
902 recordings in voltage-clamp mode were established from DL5 PNs in flies expressing Chrimson
903 in all ab4a ORNs (from *or7a-lexA*). DL5 PNs were identified based on GFP expression (from
904 *np3481-gal4*) and the presence of light-evoked responses, and their identity was confirmed after
905 the recording by processing the biocytin fill. In pilot experiments, we tested several methods for
906 optical stimulation and were unable to achieve reliable stimulation of only a single ORN axon
907 presynaptic to the recorded PN using excitation with 590 nm light from a fiber optic-coupled
908 LED (Thorlabs M590F3 with Ø200 μm fiber, 0.22 NA). Excitation of ORN terminals was very
909 sensitive to the position and angle of the optrode relative to the antennal nerve, and we found
910 large variability in the amount of light (intensity and pulse duration) required to evoke EPSCs in
911 the PN.
912 As an alternative approach, we used wide-field illumination from a 470-nm (blue) LED
913 light source (Sutter Instrument, TLED+). We delivered light pulses of 100 μs duration at 30 s trial
914 intervals, starting at very low levels of light (<0.1 mW/mm^2) and gradually increasing the light

intensity until an EPSC was observed in an all-or-none manner. At the threshold intensity, trials that fail to evoke an EPSC were infrequently interleaved with successful trials. The ORN-PN synapse is highly reliable, with a single ORN spike evoking robust release of many synaptic vesicles at the ORN terminal (Kazama and Wilson, 2008); thus, we interpret these failures as a failure to recruit a spike in a presynaptic axon on that trial (as opposed to a failure in synaptic transmission). As the light intensity was further increased, EPSC amplitude remained relatively constant, until it was observed to suddenly double, reflecting the recruitment of a second ORN axon. The mean uEPSC for each PN was determined by averaging the evoked EPSC in ~8-12 trials at a light intensity approximately halfway between the initial threshold intensity and the doubling intensity. Recordings were discarded if any of the following criteria occurred: 1) a high rate of failures at the light intensity chosen for data collection (>10%); 2) uEPSC amplitude was not stable over a range of at least ~5 μW spanning the chosen light intensity; 2) the shape of the uEPSC was not stable.

Data Analysis

Unless otherwise stated, all analyses were performed in MATLAB (Mathworks, Natick, MA).

Quantification of electrophysiological responses

Analysis of neural responses was performed masked to the experimental condition (odor- versus solvent-exposed) of the recording. For each odor stimulus measurement in a fly, a trial block was comprised of 5 stimulus presentations for ORN responses, or 6 presentations for PN responses, at an intertrial interval of 40 s. The first trial for PN responses was not included in the analysis. Spike times were determined from raw ORN and PN voltage traces using custom scripts in MATLAB that identified spikes by thresholding on the first- and second-derivatives of the voltage. All spikes were manually inspected. Spike times were converted into a peristimulus time histogram (PSTH) by counting the number of spikes in 50-ms bins, overlapping by 25 ms.

Single-trial PSTHs were averaged to generate a mean PSTH that describes the odor response for each cell. For membrane potential, single-trial voltage traces were averaged to generate a mean depolarization response for each cell. For each DL5 and VM7 PN, the response magnitude for each stimulus was computed as the trial-averaged spike rate (or membrane potential) during the 500-ms odor stimulus period, minus the trial-averaged spontaneous firing rate (or membrane potential) during the preceding 500 ms. For VA6 PNs, the response magnitude was computed over a 1000-ms window that begins at stimulus onset, which better captured the protracted odor response (which extends into the post-stimulus period) observed in this cell type. A mean response magnitude was computed across trials for each experiment, and the overall mean response was plotted as mean ± SEM across all experiments in each condition.

Analysis of LN anatomical innervation

Images of all antennal lobes were collected with identical laser power and imaging settings (magnification, detector gain, offset, pixel size, and dwell time). Brains in which >0.01% of pixels in neuropil regions (excluding cell bodies and primary neurites) were high or low saturated were rejected. Confocal image stacks were imported into ImageJ (NIH) for analysis. Analysis of LN innervation was conducted masked to the experimental condition (odor- versus solvent-exposed). The boundaries of glomeruli of interest were manually traced in every third slice using the nc82 neuropil signal, guided by published atlases (Couto et al., 2005; Laissue et al., 1999), and then interpolated through the stack to obtain the boundaries in adjacent slices. The 3D ROI manager plugin (Ollion et al., 2013) was used to group together sets of ROIs across slices corresponding to each glomerulus to define the volumetric boundaries for each glomerulus and was then used for quantification of glomerular volume (number of pixels) and pixel intensities in each channel. For each 3D ROI corresponding to an individual identified glomerulus, LN neurites or neuropil per volume was computed as the sum of the pixel values in the ROI in the

anti-CD8 (LN neurites) or nc82 (neuropil) channels, respectively, divided by the total number of pixels. The ratio of LN neurites to neuropil was computed as the sum of the pixel values in the ROI in the anti-CD8 channel divided by the sum of the pixel values in the ROI in the nc82 channel. To combine measurements across all glomeruli for a given metric (e.g. volume, LN neurites per volume, etc.), the measurement for each glomerulus in an experiment was normalized to the mean value for that glomerulus across all experiments in the solvent-exposed control condition. Plots show mean and standard error across brains.

Analysis of calcium imaging

The duration of each calcium imaging trial was 15 s, collected at 11 frames per second and 256x96 pixels per frame. Stimulus-evoked calcium signals (ΔF/F) were quantified from background-subtracted movies as the change in fluorescence ($F-F_0$) normalized to the mean fluorescence during the baseline period of each trial (F_0, averaged over 70 frames immediately preceding the odor), computed on a pixel-by-pixel basis in each frame. A Gaussian lowpass filter of size 4×4 pixels was applied to raw ΔF/F heatmaps.

A region-of-interest (ROI) was manually traced around each DL5 glomerulus, which contain the ab4a ORN terminals. ΔF/F signals were averaged across the pixels in the two DL5 ROIs and across three trials for each stimulus in an experiment. The odor response to the 500-ms stimulus presentation was typically captured in ~6 frames. The peak response for each experiment was quantified from the frame containing the maximum mean ΔF/F signal during the stimulus presentation. The overall mean response was plotted as mean ± SEM across all experiments in each condition.

Statistics

A permutation analysis was used to evaluate differences between experimental groups because of its conceptual simplicity and because it does not require assumptions about the underlying distribution of the population. For each measurement (e.g., the response of a PN type to an odor stimulus), experimental observations from flies in odor- and solvent-exposed conditions were combined and randomly reassigned into two groups (maintaining the number of samples in each respective experimental group), and the difference between the means of the groups was computed. This permutation process was repeated 10,000 times without replacement to generate a distribution for the difference between the means of the odor- and solvent-exposed groups (see Figure 2 – figure supplement 1 for an example), under the null assumption that there is no difference between the two populations. We calculated the fraction of the empirically resampled distribution which had an absolute value that equaled or exceeded the absolute observed difference between the means of the odor- and solvent-exposed groups to determine the two-tailed p-value that the observed outcome occurred by chance if the populations are not different. The cut-off for statistical significance of α=0.05 was adjusted to account for multiple comparisons in an experiment using a Bonferroni correction. Permutation testing was used in all figures, except in Figure 5 where the Mann-Whitney *U*-test was used, implemented in MATLAB (Wilcoxon rank sum test).

Sample sizes were not predetermined using a power analysis. We used sample sizes comparable to those used in similar types of studies (e.g., (Bhandawat et al., 2007; Das et al., 2011; Sachse et al., 2007)). The experimenter was not masked to experimental condition or genotype during data collection. For a subset of analyses (analysis of electrophysiological data and quantification of LN innervation), the analyst was masked to the experimental condition, as described above.

DECLARATION OF INTERESTS

The authors declare no competing interests.

ACKNOWLEDGEMENTS

We thank Chris Potter for the gift of Or7a-KI flies. We thank Meike Lobb-Rabe for generating the Or7a-lexA flies. We thank Daniel Wagenaar and the Caltech Neurotechnology Center for technical support in constructing fly holders and custom odor delivery devices. We thank members of the Hong laboratory for their critical reading and feedback on this manuscript. This work was supported by grants from the National Science Foundation (Award #1556230), the Shurl and Kay Curci Foundation, and the National Institutes of Health (1RF1MH117825). E.J.H. was supported by a Clare Boothe Luce professorship.

REFERENCES

Barlow, H.G. (1961). Possible principles underlying the transformation of sensory messages. In Sensory Communication, W.A. Rosenblith, ed. (Cambridge, MA: MIT Press), pp. 217–234.

Beaulieu, C., and Cynader, M. (1990a). Effect of the richness of the environment on neurons in cat visual cortex. I. Receptive field properties. Brain Res. Dev. Brain Res. *53*, 71–81.

Beaulieu, C., and Cynader, M. (1990b). Effect of the richness of the environment on neurons in cat visual cortex. II. Spatial and temporal frequency characteristics. Brain Res. Dev. Brain Res. *53*, 82–88.

Bhandawat, V., Olsen, S.R., Schlief, M.L., Gouwens, N.W., and Wilson, R.I. (2007). Sensory processing in the Drosophila antennal lobe increases the reliability and separability of ensemble odor representations. Nature Neuroscience *10*, 1474–1482.

Boschetti, A., Biasioli, F., van Opbergen, M., Warneke, C., Jordan, A., Holzinger, R., Prazeller, P., Karl, T., Hansel, A., Lindinger, W., et al. (1999). PTR-MS real time monitoring of the emission of volatile organic compounds during postharvest aging of berryfruit. Postharvest Biology and Technology *17*, 143–151.

de Bruyne, M., Clyne, P.J., and Carlson, J.R. (1999). Odor coding in a model olfactory organ: the Drosophila maxillary palp. J. Neurosci. *19*, 4520–4532.

de Bruyne, M., Foster, K., and Carlson, J.R. (2001). Odor coding in the Drosophila antenna. Neuron *30*, 537–552.

Cadiou, H., Aoudé, I., Tazir, B., Molinas, A., Fenech, C., Meunier, N., and Grosmaitre, X. (2014). Postnatal Odorant Exposure Induces Peripheral Olfactory Plasticity at the Cellular Level. J. Neurosci. *34*, 4857–4870.

Cafaro, J. (2016). Multiple sites of adaptation lead to contrast encoding in the Drosophila olfactory system. Physiological Reports *4*, e12762.

Cang, J., and Feldheim, D.A. (2013). Developmental Mechanisms of Topographic Map Formation and Alignment. Annual Review of Neuroscience *36*, 51–77.

Cavallin, M.A., Powell, K., Biju, K.C., and Fadool, D.A. (2010). State-dependent sculpting of olfactory sensory neurons is attributed to sensory enrichment, odor deprivation, and aging. Neurosci. Lett. *483*, 90–95.

Chakraborty, T.S., Goswami, S.P., and Siddiqi, O. (2009). Sensory Correlates of Imaginal Conditioning in Drosophila melanogaster. Journal of Neurogenetics *23*, 210–219.

Chan, Y.-C., and Chiao, C.-C. (2008). Effect of visual experience on the maturation of ON–OFF direction selective ganglion cells in the rabbit retina. Vision Research *48*, 2466–2475.

Chen, T.W., Wardill, T.J., Sun, Y., Pulver, S.R., Renninger, S.L., Baohan, A., Schreiter, E.R., Kerr, R.A., Orger, M.B., Jayaraman, V., et al. (2013). Ultrasensitive fluorescent proteins for imaging neuronal activity. Nature *499*, 295–300.

Chodankar, A., Sadanandappa, M.K., VijayRaghavan, K., and Ramaswami, M. (2020). Glomerulus-Selective Regulation of a Critical Period for Interneuron Plasticity in the Drosophila Antennal Lobe. J. Neurosci. *40*, 5549–5560.

Couto, A., Alenius, M., and Dickson, B.J. (2005). Molecular, anatomical, and functional organization of the Drosophila olfactory system. Current Biology *15*, 1535–1547.

Das, A., Sen, S., Lichtneckert, R., Okada, R., Ito, K., Rodrigues, V., and Reichert, H. (2008). Drosophila olfactory local interneurons and projection neurons derive from a common neuroblast lineage specified by the empty spiracles gene. Neural Dev. *3*, 33.

Das, S., Sadanandappa, M.K., Dervan, A., Larkin, A., Lee, J.A., Sudhakaran, I.P., Priya, R., Heidari, R., Holohan, E.E., Pimentel, A., et al. (2011). Plasticity of local GABAergic interneurons drives olfactory habituation. Proc Natl Acad Sci U S A *108*, E646–E654.

Devaud, J.M., and Ferrus, A. (2003). Molecular genetics of activity-dependent structural changes at the synapse. Journal of Neurogenetics *17*, 271–293.

Devaud, J.M., Acebes, A., and Ferrus, A. (2001). Odor exposure causes central adaptation and morphological changes in selected olfactory glomeruli in Drosophila. The Journal of Neuroscience : The Official Journal of the Society for Neuroscience *21*, 6274–6282.

1078 Devaud, J.M., Acebes, A., Ramaswami, M., and Ferrus, A. (2003). Structural and functional
1079 changes in the olfactory pathway of adult Drosophila take place at a critical age. Journal of
1080 Neurobiology *56*, 13–23.

1081 D'Orazi, F.D., Suzuki, S.C., and Wong, R.O. (2014). Neuronal remodeling in retinal circuit
1082 assembly, disassembly, and reassembly. Trends in Neurosciences *37*, 594–603.

1083 Elstrott, J., and Feller, M.B. (2009). Vision and the establishment of direction-selectivity: a tale
1084 of two circuits. Current Opinion in Neurobiology *19*, 293–297.

1085 Elstrott, J., Anishchenko, A., Greschner, M., Sher, A., Litke, A.M., Chichilnisky, E.J., and Feller,
1086 M.B. (2008). Direction Selectivity in the Retina Is Established Independent of Visual Experience
1087 and Cholinergic Retinal Waves. Neuron *58*, 499–506.

1088 Engineer, N.D., Percaccio, C.R., Pandya, P.K., Moucha, R., Rathbun, D.L., and Kilgard, M.P.
1089 (2004). Environmental Enrichment Improves Response Strength, Threshold, Selectivity, and
1090 Latency of Auditory Cortex Neurons. Journal of Neurophysiology *92*, 73–82.

1091 Espinosa, J.S., and Stryker, M.P. (2012). Development and Plasticity of the Primary Visual
1092 Cortex. Neuron *75*, 230–249.

1093 Farneti, B., Khomenko, I., Grisenti, M., Ajelli, M., Betta, E., Algarra, A.A., Cappellin, L., Aprea,
1094 E., Gasperi, F., Biasioli, F., et al. (2017). Exploring Blueberry Aroma Complexity by
1095 Chromatographic and Direct-Injection Spectrometric Techniques. Front. Plant Sci. *8*.

1096 Fiser, J., Berkes, P., Orban, G., and Lengyel, M. (2010). Statistically optimal perception and
1097 learning: from behavior to neural representations. Trends in Cognitive Sciences *14*, 119–130.

1098 Fishilevich, E., and Vosshall, L.B. (2005). Genetic and functional subdivision of the Drosophila
1099 antennal lobe. Current Biology *15*, 1548–1553.

1100 Fouquet, W., Owald, D., Wichmann, C., Mertel, S., Depner, H., Dyba, M., Hallermann, S., Kittel,
1101 R.J., Eimer, S., and Sigrist, S.J. (2009). Maturation of active zone assembly by Drosophila
1102 Bruchpilot. Journal of Cell Biology *186*, 129–145.

1103 Gilbert, C.D., Li, W., and Piech, V. (2009). Perceptual learning and adult cortical plasticity. The
1104 Journal of Physiology *587*, 2743–2751.

1105 Golovin, R.M., and Broadie, K. (2016). Developmental experience-dependent plasticity in the
1106 first synapse of the Drosophila olfactory circuit. J Neurophysiol *116*, 2730–2738.

1107 Golovin, R.M., Vest, J., Vita, D.J., and Broadie, K. (2019). Activity-Dependent Remodeling of
1108 Drosophila Olfactory Sensory Neuron Brain Innervation during an Early-Life Critical Period. J.
1109 Neurosci. *39*, 2995–3012.

1110 Grabe, V., Baschwitz, A., Dweck, H.K.M., Lavista-Llanos, S., Hansson, B.S., and Sachse, S.
1111 (2016). Elucidating the Neuronal Architecture of Olfactory Glomeruli in the Drosophila Antennal
1112 Lobe. Cell Reports *16*, 3401–3413.

1113 Hallem, E.A., and Carlson, J.R. (2006). Coding of odors by a receptor repertoire. Cell *125*, 143–
1114 160.

1115 Hallem, E.A., Ho, M.G., and Carlson, J.R. (2004). The molecular basis of odor coding in the
1116 Drosophila antenna. Cell *117*, 965–979.

1117 Hayashi, S., Ito, K., Sado, Y., Taniguchi, M., Akimoto, A., Takeuchi, H., Aigaki, T., Matsuzaki,
1118 F., Nakagoshi, H., Tanimura, T., et al. (2002). GETDB, a database compiling expression
1119 patterns and molecular locations of a collection of gal4 enhancer traps. Genesis *34*, 58–61.

1120 Heisenberg, M. (2003). Mushroom body memoir: from maps to models. Nature Reviews.
1121 Neuroscience *4*, 266–275.

1122 Hong, E.J., and Wilson, R.I. (2015). Simultaneous encoding of odors by channels with diverse
1123 sensitivity to inhibition. Neuron *85*, 573–589.

1124 Horne, J.A., Langille, C., McLin, S., Wiederman, M., Lu, Z., Xu, C.S., Plaza, S.M., Scheffer, L.K.,
1125 Hess, H.F., and Meinertzhagen, I.A. (2018). A resource for the Drosophila antennal lobe
1126 provided by the connectome of glomerulus VA1v. ELife *7*, e37550.

1127 Huberman, A.D., Feller, M.B., and Chapman, B. (2008). Mechanisms Underlying Development
1128 of Visual Maps and Receptive Fields. Annual Review of Neuroscience *31*, 479–509.

1129 Iyengar, A., Chakraborty, T.S., Goswami, S.P., Wu, C.-F., and Siddiqi, O. (2010). Post-eclosion
1130 odor experience modifies olfactory receptor neuron coding in Drosophila. PNAS *107*, 9855–
1131 9860.

1132 Jeanne, J.M., and Wilson, R.I. (2015). Convergence, Divergence, and Reconvergence in a
1133 Feedforward Network Improves Neural Speed and Accuracy. Neuron *88*, 1014–1026.

1134 Jones, S.V., Choi, D.C., Davis, M., and Ressler, K.J. (2008). Learning-dependent structural
1135 plasticity in the adult olfactory pathway. J. Neurosci. *28*, 13106–13111.

1136 Jordán, M.J., Tandon, K., Shaw, P.E., and Goodner, K.L. (2001). Aromatic Profile of Aqueous
1137 Banana Essence and Banana Fruit by Gas Chromatography−Mass Spectrometry (GC-MS) and
1138 Gas Chromatography−Olfactometry (GC-O). J. Agric. Food Chem. *49*, 4813–4817.

1139 Kass, M.D., Moberly, A.H., Rosenthal, M.C., Guang, S.A., and McGann, J.P. (2013). Odor-
1140 Specific, Olfactory Marker Protein-Mediated Sparsening of Primary Olfactory Input to the Brain
1141 after Odor Exposure. J. Neurosci. *33*, 6594–6602.

1142 Kazama, H., and Wilson, R.I. (2008). Homeostatic matching and nonlinear amplification at
1143 genetically-identified central synapses. Neuron *58*, 401–413.

1144 Kazama, H., Yaksi, E., and Wilson, R.I. (2011). Cell death triggers olfactory circuit plasticity via
1145 glial signaling in Drosophila. The Journal of Neuroscience : The Official Journal of the Society
1146 for Neuroscience *31*, 7619–7630.

1147 Kidd, S., and Lieber, T. (2016). Mechanism of Notch Pathway Activation and Its Role in the
1148 Regulation of Olfactory Plasticity in Drosophila melanogaster. PLOS ONE *11*, e0151279.

1149 Kidd, S., Struhl, G., and Lieber, T. (2015). Notch is required in adult Drosophila sensory
1150 neurons for morphological and functional plasticity of the olfactory circuit. PLoS Genetics *11*,
1151 e1005244.

1152 Kim, S., Chen, J., Cheng, T., Gindulyte, A., He, J., He, S., Li, Q., Shoemaker, B.A., Thiessen,
1153 P.A., Yu, B., et al. (2021). PubChem in 2021: new data content and improved web interfaces.
1154 Nucleic Acids Research *49*, D1388–D1395.

1155 Klapoetke, N.C., Murata, Y., Kim, S.S., Pulver, S.R., Birdsey-Benson, A., Cho, Y.K., Morimoto,
1156 T.K., Chuong, A.S., Carpenter, E.J., Tian, Z., et al. (2014). Independent optical excitation of
1157 distinct neural populations. Nature Methods *11*, 338–346.

1158 Kreile, A.K., Bonhoeffer, T., and Hübener, M. (2011). Altered Visual Experience Induces
1159 Instructive Changes of Orientation Preference in Mouse Visual Cortex. J Neurosci *31*, 13911–
1160 13920.

1161 Laissue, P.P., Reiter, C., Hiesinger, P.R., Halter, S., Fischbach, K.F., and Stocker, R.F. (1999).
1162 Three-dimensional reconstruction of the antennal lobe in Drosophila melanogaster. Journal of
1163 Comparative Neurology *405*, 543–552.

1164 Lee, T., and Luo, L. (1999). Mosaic analysis with a repressible cell marker for studies of gene
1165 function in neuronal morphogenesis. Neuron *22*, 451–461.

1166 Li, Y., Fitzpatrick, D., and White, L.E. (2006). The development of direction selectivity in ferret
1167 visual cortex requires early visual experience. Nat Neurosci *9*, 676–681.

1168 Li, Y., Hooser, S.D.V., Mazurek, M., White, L.E., and Fitzpatrick, D. (2008). Experience with
1169 moving visual stimuli drives the early development of cortical direction selectivity. Nature *456*,
1170 952–956.

1171 Lin, C.-C., Prokop-Prigge, K.A., Preti, G., and Potter, C.J. (2015). Food odors trigger
1172 Drosophila males to deposit a pheromone that guides aggregation and female oviposition
1173 decisions. ELife *4*, e08688.

1174 Liu, A., and Urban, N.N. (2017). Prenatal and Early Postnatal Odorant Exposure Heightens
1175 Odor-Evoked Mitral Cell Responses in the Mouse Olfactory Bulb. ENeuro *4*.

1176 Liu, A., Savya, S., and Urban, N.N. (2016). Early Odorant Exposure Increases the Number of
1177 Mitral and Tufted Cells Associated with a Single Glomerulus. J. Neurosci. *36*, 11646–11653.

1178 Mandairon, N., and Linster, C. (2009). Odor Perception and Olfactory Bulb Plasticity in Adult
1179 Mammals. Journal of Neurophysiology *101*, 2204–2209.

1180 Mandairon, N., Stack, C., Kiselycznyk, C., and Linster, C. (2006a). Enrichment to odors
1181 improves olfactory discrimination in adult rats. Behav Neurosci *120*, 173–179.

1182 Mandairon, N., Stack, C., Kiselycznyk, C., and Linster, C. (2006b). Broad activation of the
1183 olfactory bulb produces long-lasting changes in odor perception. PNAS *103*, 13543–13548.

1184 Marin, E.C., Watts, R.J., Tanaka, N.K., Ito, K., and Luo, L. (2005). Developmentally
1185 programmed remodeling of the Drosophila olfactory circuit. Development *132*, 725–737.

1186 Martelli, C., and Fiala, A. (2019). Slow presynaptic mechanisms that mediate adaptation in the
1187 olfactory pathway of Drosophila. ELife *8*, e43735.

1188 Moore, J.K., and Linthicum, F.H. (2007). The human auditory system: A timeline of
1189 development. International Journal of Audiology *46*, 460–478.

1190 Nagel, K.I., and Wilson, R.I. (2011). Biophysical mechanisms underlying olfactory receptor
1191 neuron dynamics. Nature Neuroscience *14*, 208–216.

1192 National Institute for Occupational Safety and Health (NIOSH), Centers for Disease Control and
1193 1197 Prevention (CDC). "Immediately Dangerous to Life or Health (IDLH) Values," 2019,
1194 1198 https://www.cdc.gov/niosh/idlh/, Accessed 11 Oct 2020
1195
1196 Ollion, J., Cochennec, J., Loll, F., Escudé, C., and Boudier, T. (2013). TANGO: a generic tool for
1197 high-throughput 3D image analysis for studying nuclear organization. Bioinformatics *29*, 1840–
1198 1841.

1199 Olsen, S.R., and Wilson, R.I. (2008). Lateral presynaptic inhibition mediates gain control in an
1200 olfactory circuit. Nature *452*, 956–960.

1201 Olsen, S.R., Bhandawat, V., and Wilson, R.I. (2007). Excitatory interactions between olfactory
1202 processing channels in the Drosophila antennal lobe. Neuron *54*, 89–103.

1203 Olsen, S.R., Bhandawat, V., and Wilson, R.I. (2010). Divisive normalization in olfactory
1204 population codes. Neuron *66*, 287–299.

1205 Pech, U., Revelo, N.H., Seitz, K.J., Rizzoli, S.O., and Fiala, A. (2015). Optical Dissection of
1206 Experience-Dependent Pre- and Postsynaptic Plasticity in the Drosophila Brain. Cell Reports
1207 *10*, 2083–2095.

1208 Pfeiffer, B.D., Ngo, T.T., Hibbard, K.L., Murphy, C., Jenett, A., Truman, J.W., and Rubin, G.M.
1209 (2010). Refinement of tools for targeted gene expression in Drosophila. Genetics *186*, 735–755.

1210 Pienkowski, M., and Eggermont, J.J. (2011). Cortical tonotopic map plasticity and behavior.
1211 Neurosci Biobehav Rev *35*, 2117–2128.

1212 Ressler, K.J., Sullivan, S.L., and Buck, L.B. (1994). Information coding in the olfactory system:
1213 evidence for a stereotyped and highly organized epitope map in the olfactory bulb. Cell *79*,
1214 1245–1255.

1215 Rochefort, C., Gheusi, G., Vincent, J.-D., and Lledo, P.-M. (2002). Enriched Odor Exposure
1216 Increases the Number of Newborn Neurons in the Adult Olfactory Bulb and Improves Odor
1217 Memory. J. Neurosci. *22*, 2679–2689.

1218 Root, C.M., Semmelhack, J.L., Wong, A.M., Flores, J., and Wang, J.W. (2007). Propagation of
1219 olfactory information in Drosophila. Proceedings of the National Academy of Sciences of the
1220 United States of America *104*, 11826–11831.

1221 Rybak, J., Talarico, G., Ruiz, S., Arnold, C., Cantera, R., and Hansson, B.S. (2016). Synaptic
1222 circuitry of identified neurons in the antennal lobe of Drosophila melanogaster. Journal of
1223 Comparative Neurology *524*, 1920–1956.

1224 Sachse, S., Rueckert, E., Keller, A., Okada, R., Tanaka, N.K., Ito, K., and Vosshall, L.B. (2007).
1225 Activity-dependent plasticity in an olfactory circuit. Neuron *56*, 838–850.

1226 Sanes, D.H., and Bao, S. (2009). Tuning up the Developing Auditory CNS. Curr Opin Neurobiol
1227 *19*, 188–199.

1228 Santoro, S.W., and Dulac, C. (2012). The activity-dependent histone variant H2BE modulates
1229 the life span of olfactory neurons. Elife *1*, e00070.

1230 Schlief, M.L., and Wilson, R.I. (2007). Olfactory processing and behavior downstream from
1231 highly selective receptor neurons. Nature Neuroscience *10*, 623–630.

1232 Sengpiel, F., Stawinski, P., and Bonhoeffer, T. (1999). Influence of experience on orientation
1233 maps in cat visual cortex. Nat Neurosci *2*, 727–732.

1234 Shang, Y., Claridge-Chang, A., Sjulson, L., Pypaert, M., and Miesenbock, G. (2007). Excitatory
1235 local circuits and their implications for olfactory processing in the fly antennal lobe. Cell *128*,
1236 601–612.

1237 Silbering, A.F., Rytz, R., Grosjean, Y., Abuin, L., Ramdya, P., Jefferis, G.S., and Benton, R.
1238 (2011). Complementary function and integrated wiring of the evolutionarily distinct Drosophila
1239 olfactory subsystems. The Journal of Neuroscience : The Official Journal of the Society for
1240 Neuroscience *31*, 13357–13375.

1241 Steinemann, A. (2016). Fragranced consumer products: exposures and effects from emissions.
1242 Air Qual Atmos Health *9*, 861–866.

1243 Stocker, R.F., Lienhard, M.C., Borst, A., and Fischbach, K.F. (1990). Neuronal architecture of
1244 the antennal lobe in Drosophila melanogaster. Cell and Tissue Research *262*, 9–34.

1245 Tobin, W.F., Wilson, R.I., and Lee, W.-C.A. (2017). Wiring variations that enable and constrain
1246 neural computation in a sensory microcircuit. ELife *6*, e24838.

1247 Todrank, J., Heth, G., and Restrepo, D. (2011). Effects of in utero odorant exposure on
1248 neuroanatomical development of the olfactory bulb and odour preferences. Proc Biol Sci *278*,
1249 1949–1955.

1250 Vassar, R., Chao, S.K., Sitcheran, R., Nunez, J.M., Vosshall, L.B., and Axel, R. (1994).
1251 Topographic organization of sensory projections to the olfactory bulb. Cell *79*, 981–991.

1252 Vosshall, L.B., and Stocker, R.F. (2007). Molecular architecture of smell and taste in
1253 Drosophila. Annu Rev Neurosci *30*, 505–533.

1254 Vosshall, L.B., Wong, A.M., and Axel, R. (2000). An olfactory sensory map in the fly brain. Cell
1255 *102*, 147–159.

Wang, H.W., Wysocki, C.J., and Gold, G.H. (1993). Induction of olfactory receptor sensitivity in mice. Science *260*, 998–1000.

Watt, W.C., Sakano, H., Lee, Z.-Y., Reusch, J.E., Trinh, K., and Storm, D.R. (2004). Odorant stimulation enhances survival of olfactory sensory neurons via MAPK and CREB. Neuron *41*, 955–967.

Wilson, R.I. (2013). Early olfactory processing in Drosophila: mechanisms and principles. Annual Review of Neuroscience *36*, in press.

Wilson, D.A., Sullivan, R.M., and Leon, M. (1985). Odor Familiarity Alters Mitral Cell Response in the Olfactory Bulb of Neonatal Rats. Developmental Brain Research *22*, 314–317.

Wilson, R.I., Turner, G.C., and Laurent, G. (2004). Transformation of olfactory representations in the Drosophila antennal lobe. Science *303*, 366–370.

Wolkoff, P., and Nielsen, G.D. (2017). Effects by inhalation of abundant fragrances in indoor air – An overview. Environment International *101*, 96–107.

Woo, C.C., Hingco, E.E., Taylor, G.E., and Leon, M. (2006). Exposure to a broad range of odorants decreases cell mortality in the olfactory bulb. Neuroreport *17*, 817–821.

Wypych, G. (2017). Handbook of Odors in Plastic Materials (Elsevier).

Yaksi, E., and Wilson, R.I. (2010). Electrical coupling between olfactory glomeruli. Neuron *67*, 1034–1047.

Zhang, L.I., Bao, S., and Merzenich, M.M. (2001). Persistent and specific influences of early acoustic environments on primary auditory cortex. Nat Neurosci *4*, 1123–1130.